Competing local warming and large-scale cooling effects of reducing terrestrial evaporation: lessons from Northland, a planet with a hemispheric continent

Marysa M. Laguë*

Department of Earth and Planetary Science, University of California Berkeley, Berkeley, CA, USA

Marianne Pietschnig

Department of Mathematics, University of Exeter, Exeter, United Kingdom

Sarah Ragen

School of Oceanography, University of Washington, Seattle, WA, USA

Timothy A. Smith

Oden Institute for Computational Engineering and Sciences, The University of Texas at Austin, Austin, TX, USA

David S. Battisti

Department of Atmospheric Sciences, University of Washington, Seattle, WA, USA

* *Corresponding author address:* Marysa M. Laguë, Department of Earth and Planetary Science, University of California Berkeley, 307 McCone Hall, Berkeley, CA 94720.

E-mail: mlague@berkeley.edu

ABSTRACT

Motivated by the hemispheric asymmetry of land distribution on Earth, we explore the climate of Northland, a highly idealized planet with a Northern Hemisphere continent and a Southern Hemisphere ocean. We evaluate how modifying land surface properties on Northland drives changes in temperatures, precipitation patterns, the global energy budget, and atmospheric dynamics. We observe surprising results in response to changes in land-surface evaporation, where suppressing terrestrial evaporation in Northland cools both land and ocean. In previous studies, suppressing terrestrial evaporation has been found to lead to local warming by reducing latent cooling of the land surface. However, reduced evaporation can also decrease atmospheric water vapor, reducing the strength of the greenhouse effect and leading to large-scale cooling. Here, we use a set of idealized climate model simulations to show that suppressing terrestrial evaporation over Northern Hemisphere continents of varying size can lead to either warming or cooling of the land surface, depending on which of these competing effects dominate. We find that a combination of total land area and contiguous continent size control the balance between local warming from reduced latent heat flux and large-scale cooling from reduced atmospheric water vapor. The climate of Northland can be separated into four distinct regions: the Southern Hemisphere ocean, the seasonally wet tropics, the mid-latitude desert, and the Great Northern Swamp. We demonstrate how terrestrial heat capacity, albedo, and evaporation all modulate the location of the ITCZ both over the continent and over the ocean.

1. Introduction

The physical properties of the land surface and the ocean differ in several fundamental ways. For instance, land has a much lower heat capacity than ocean (Cess and Goldenberg 1981; North et al. 1983; Bonan 2008); land has a higher albedo than ocean (Budyko 1961, 1969; Payne 1972; Bonan 2008); the ocean has the ability to move heat laterally (Loft 1918; Richardson 1980; Trenberth and Caron 2001; Ferrari and Ferreira 2011; Forget and Ferreira 2019); and there are large climatic impacts of terrestrial orography (Queney 1948; Eliassen and Palm 1960; Manabe and Terpstra 1974; Held et al. 1985; McFarlane 1987). Moreover, land stores and evaporates less water than ocean, and soil and vegetation properties provide resistance to evaporation over land (Manabe 1969; Bonan 2008, and references therein). The contrast between physical properties of land and ocean are important controls on atmospheric dynamics, profoundly impacting the climate. The hemispheric asymmetry in land-sea distribution has implications for global climate, including the higher sensitivity of the Northern Hemisphere to increases in anthropogenic greenhouse gases (Manabe et al. 1991; Stouffer et al. 1989). In this study, we focus on how the limited capacity of the land to hold water, its small heat capacity, and its higher albedo alter the climate system.

The albedo of different land types is much higher than that of ice-free ocean. Land albedo ranges from 0.05-0.25 (vegetated) to 0.5-0.9 (glaciers and snow) (Wiscombe and Warren 1980; Oke 1987; Bonan 2008). In contrast, the surface albedo of the ice-free ocean is generally less than 0.1 (Jin et al. 2004). The difference in top-of-atmosphere (TOA) albedo between land and ocean is less drastic, with TOA albedo ranging from 0.25 to 0.6 over snow-free land, and 0.1 to 0.5 over ice-free ocean for Earth in the present climate. These higher values result from atmospheric controls on the TOA albedo, via the effects of cloud cover, aerosols, and attenuation (Donohoe and Battisti 2011).

Additionally, land has a much smaller heat capacity than the ocean, and a limited ability to move energy laterally. Oceans can absorb large amounts of energy (Kuhlbrodt and Gregory 2012; Cheng et al. 2017) and transport energy via ocean currents; there are areas of the ocean that can continually take up energy, while other regions act as a source of energy to the atmosphere (e.g. Marshall and Zanna 2014; Forget and Ferreira 2019). In contrast, energy absorbed at one location on land must be released back to the atmosphere at that same location in the form of upwards longwave radiation, sensible heat, or latent heat (evaporation). While the land can store energy on seasonal timescales, the annual mean heat storage of a land surface in equilibrium is near-zero (Milly and Shmakin 2002), and the seasonal storage of heat by the land surface is much smaller than that of the ocean (Marshall and Plumb 2008).

The limited capacity of the land surface to hold water and the increased resistance to evaporation over land surfaces compared to over open water drastically alters evaporative fluxes over land. Over the ocean, evaporation is determined mainly by the meteorological conditions at the atmosphere-ocean interface (e.g. the surface temperature and atmospheric humidity). In contrast, dry land surfaces have little water available for evaporation, and thus little evaporation occurs regardless of the evaporative demand of the overlying atmosphere. Various properties of soil and vegetation further modulate the availability of water to the atmosphere, including total leaf area and roots that can provide access to water deep in the soil column (Canadell et al. 1996; Bonan 2008). Moreover, plants directly regulate the movement of water from the land to the atmosphere by opening and closing their stomata (small pores on leaves which modulate gas exchange) (Sellers et al. 1996).

These fundamental physical differences between land and ocean result in very different surface-atmosphere interactions. Changes in land surface properties can modify the global climate system (Charney 1975; Shukla and Mintz 1982; Sud et al. 1988; Davin et al. 2010; Laguë et al. 2019).

Large hemispheric energy imbalances, such as those generated by sea ice, large-scale vegetation change, or an idealized energy source can drive large-scale changes in the location of the zonal mean ITCZ and the Hadley circulation (Chiang and Bitz 2005; Broccoli et al. 2006; Kang et al. 2008; Swann et al. 2012; Laguë and Swann 2016; Kang 2020). In response to a hemispheric energy imbalance, the rising branch of the Hadley circulation moves towards the energy-rich hemisphere, thereby moving energy towards the energy-poor hemisphere and shifting the ITCZ towards the energy-rich hemisphere (Donohoe et al. 2013), provided there are no large changes in gross moist stability (see Geen et al. 2020, and references therein). The distribution of land impacts climate in myriad ways, including by directing storm tracks, shaping ocean circulation, generating planetary waves, and impacting orographic forcing and diabatic heating of the atmosphere (Eliassen and Palm 1960; Hartmann 1994; Donohoe et al. 2020). In this study we investigate the fundamental differences in atmospheric dynamics and climate over land and ocean, as well as the climatic implications of the asymmetry in the distribution of land between the Southern Hemisphere (SH) and the Northern Hemisphere (NH).

This study explores the climate of an idealized limit of the distribution of the land-ocean system. At present, 68% of land on Earth is in the NH and 32% is in the SH. The hemispheric asymmetry in this distribution of land has long been thought to drive asymmetries in surface temperature (Croll 1870; Stouffer et al. 1989; Manabe et al. 1991), precipitation and ocean heat transport (Nilsson et al. 2013).

In this study, we use an idealized atmospheric general circulation model configuration to explore how fundamental differences between the land and ocean affect the climate. To do this, we model the climate of a hypothetical planet that is Earth-like in size and orbital configuration, but has a continent covering the entire Northern Hemisphere, and an ocean covering the entire Southern Hemisphere. We explore the mean state of this planet, which we call Northland, and probe how

modifying the albedo and capacity to hold water of the land surface alter the planet's climate. We also explore the climate of several alternative continental configurations, and consider a land-covered planet.

Idealized models are a useful tool in climate modeling as they help to narrow the gap between simulating the climate system and understanding its mechanisms, as highlighted in Sellers (1969), Held (2005), Jeevanjee et al. (2017), and Maher et al. (2019). Idealized models can be traced back to 'Galilean' idealizations, in which a problem is simplified to make it easier to solve (McMullin 1985). While an idealized model sacrifices realistic representations of physical processes, this approach aides in illuminating fundamental processes of the climate system (Levins 1966) - in this case, differences between land and ocean surface interactions with the atmosphere.

2. Methods

a. Model

We use Isca (Vallis et al. 2018), a framework for designing idealized atmospheric general circulation models (GCMs) to explore the climate of an Earth-like planet with an idealized continental configuration. The atmosphere is coupled to a 20m slab ocean without any ocean heat transport in our simulations. Land gridcells differ from ocean gridcells by having a higher albedo, smaller heat capacity, a finite reservoir of water, and a parameterized representation of soil that reduces the rate of evaporation when the soil is less than saturated. The land parameterization used in this study is similar to that of Manabe (1969), where land hydrology is represented using a bucket model. In this model configuration, there is no snow or sea ice, thus no representation of surface albedo feedbacks; soil moisture does not impact land surface albedo.

The atmosphere uses moist dynamics, but does not represent clouds. While cloud responses to land surface properties and their changes can play an important role in determining impacts on surface climate (Cho et al. 2018; Sikma and Vilà-Guerau de Arellano 2019; Laguë et al. 2019; Kim et al. 2020), cloud responses to climate perturbations are also a large source of uncertainty (Stocker et al. 2013; Zelinka et al. 2017). Our idealized modeling framework avoids uncertainties associated with cloud responses to climate perturbations, at the cost of not capturing any cloud interaction effects. The surface albedo α of both water ($\alpha_{ocean} = 0.25$) and land ($\alpha_{land} = 0.325$; table 1) is higher than it would be in a model that included clouds, to allow for a more realistic planetary albedo at the top of the atmosphere (Donohoe and Battisti 2011). Despite the absence of clouds, the model still produces precipitation (see Vallis et al. 2018, for details). Simulations are run using a T42 horizontal resolution (roughly 2.8° latitude by 2.8° longitude) with 40 vertical levels.

b. Experiments

We run a total of 14 simulations, with six continental configurations and various land surface properties modified between simulations (table 1). In all simulations, there is a seasonal cycle in insolation (obliquity = 23.439 degrees, eccentricity = 0) with a 360 day year; atmospheric CO_2 concentrations are fixed at 300 ppm.

We refer to the six continental configurations as "Northland", "ThreeQuarterLand","NorthWestLand","ThreePatchLand","TwoPatchLand", and "Lakeworld", (figure 1). All configurations except Lakeworld have ocean in the SH. In the Northland configuration, the whole NH is land. ThreeQuarterLand has land only in the the NH from 90-360° longitude (thus spanning 3/4 of the Northern Hemisphere) and ocean from 0-90° longitude. NorthWestLand has land only in the NH from 180-360° longitude. ThreePatchLand has the same land area

as ThreeQuarterLand, but with three equally-spaced 90° longitude wide continents in the NH, separated by 30° longitude ocean basins. TwoPatchLand has two equally-spaced 90° longitude continents, separated by two 90° longitude ocean basins, and the total land area is the same as in NorthWestLand. In the Lakeworld configuration, the whole world is land, with no ocean. There is also an aquaplanet configuration with no land.

For the Northland continental configuration, we consider 4 simulations with varied land surface properties; we refer to these simulations as "NorthlandXX" (where "XX" indicates a specific simulation). Our "control" simulation (to which we generally compare our other experiments) is "NorthlandBright". In NorthlandBright, the NH continent has an albedo that is 1.3 times that of the ocean ($\alpha_{land} = 0.325$, $\alpha_{ocean} = 0.25$). The heat capacity of the land is 1/10 that of the ocean in our simulations (i.e. equivalent to a 2m mixed layer ocean). This is larger than the heat capacity of land on Earth, but Isca simulations with realistic continents have been shown to compare well with reanalyses when these heat capacities are used (Thomson and Vallis 2019; Geen et al. 2018). The roughness length is 0.2 mm, and is uniform over land and ocean in our simulations. Hydrology is represented by the "bucket model" (Manabe 1969; Vallis et al. 2018), where the capacity of the land to hold water ("bucket capacity") is set to 150 mm in our simulations, and water on land is initialized everywhere at 100 mm. The bucket receives water when precipitation exceeds evaporation and loses water when the opposite occurs. When the bucket is more than 3/4 full, the resistance to evaporating water from the land surface is the same as over open water. When the bucket is less than 3/4 full, evaporative resistance scales inversely with the amount of water in the bucket.

We run three additional Northland experiments to demonstrate various aspects of the land surface's impact on the climate system. In each of these simulations, a single property of the land surface is modified compared to NorthlandBright. In the "NorthlandDark" experiment, the albedo

of the land is reduced so that it is the same as the ocean ($\alpha_{land} = \alpha_{ocean} = 0.25$). In the "NorthlandEmpty" experiment, the land surface is initialized with no water on the land surface; thus, all water that ends up on land must have originated from the SH ocean. NorthlandEmpty differs from NorthlandBright only in the initial conditions. In the "NorthlandDry" experiment, the capacity of the land to hold water is greatly reduced, to near-zero (0.01 mm). This effectively shuts off evaporation from the land surface.

For each of the NorthWestLand, ThreeQuarterLand, TwoPatchLand, and ThreePatchLand continental configurations, we run two simulations. In "NorthWestLand", "ThreeQuarterLand", "TwoPatchLand", and "ThreePatchLand", the land surface has the same properties as NorthlandBright. In "NorthWestLandDry", "ThreeQuarterLandDry", "TwoPatchLandDry", and "ThreePatchLandDry", the land surface has the same properties as NorthlandDry (i.e. terrestrial evaporation is suppressed).

We run one simulation where the entire planet is covered with land. We refer to this simulation as "Lakeworld". Lakeworld has the same albedo as NorthlandBright ($\alpha_{land} = 0.325$), but the bucket hydrology is modified to allow the land to form lakes over gridcells that receive precipitation when the soil moisture bucket is already full. When the soil moisture is less than 150 mm, the same rules governing terrestrial evaporation in NorthlandBright apply. However, the soil is allowed to accumulate an infinite amount of water. When the soil moisture exceeds 150 mm, the same rules of evaporation for fully saturated soils (which in these simulations are the same as the rules for open water) apply. The lakes do not impact land albedo or heat capacity. Lastly, we run an aquaplanet simulation ("Aqua") with no land, where the whole planet is covered with a 20m deep mixed layer slab ocean, with an albedo of $\alpha_{ocean} = 0.25$.

Most simulations were run for 20 years, though some Northland simulations were run for 50 years to check model drift, and Lakeworld was run for 80 years due to the unique water cycle of

the all-land planet. The first four years of each simulation are discarded to allow for model spin-up, after which time there is a global-mean drift in surface temperatures of less than 0.01 K/year in the Northland and Aqua simulations (figure S1). Unless otherwise stated, the results presented here are taken from years 5-20 of the simulations (5-80 for Lakeworld). The Lakeworld simulation does not reach equilibrium in 80 years (figure S1), but this simulation is used to demonstrate the transient migration of water, rather than explored for its equilibrium climate.

When statistical significance is shown for a difference between two experiments, a student's t-test is used, with $p < 0.05$ indicating 95% confidence that the simulations differ significantly. When error bars are used, they represent $\pm$ 1 standard deviation.

3. Results

Here our goal is to explore the factors that control the surface energy and hydrologic budgets of the idealized Northland planet. We begin with an overview of the climatology in the Northland-Bright experiment (section a), which we view as a control simulation. We then investigate how changes in land albedo (section b) and terrestrial evaporation (section c) impact the temperature and water cycle of the planet. Next, we explore the effect of suppressing terrestrial evaporation with alternate configurations that include some ocean in the NH (section d). Finally, we explore the role of moisture transport (section e), and show that the mere presence of a continent causes the ITCZ to extend farther poleward than in a pure aquaplanet setting (section f).

a. NorthlandBright (control simulation) climatology

NorthlandBright can be divided into four distinct climatic zones: the SH ocean, the seasonally wet tropical land belt, the NH mid-latitude desert, and the NH moist polar region. The mean climate of the NorthlandBright simulation reflects a world where the area-weighted annual mean

surface temperature over the continent is slightly cooler (277K) than over the ocean (280K) (table S1); this is unlike present-day Earth, where – in the extra-tropics – land regions are generally slightly warmer than ocean regions (Wallace et al. 1995; Sutton et al. 2007). However, the continent has a much larger seasonal cycle of temperature than the ocean, reflecting its smaller heat capacity (figures 2, table S1). The hottest part of the continent, with temperatures reaching 304K, occurs around 30°N during NH summer, while temperatures near the North Pole plunge to 220K during NH winter (figure 2a). Temperatures and seasonality over the SH ocean are much more moderate, with a hemispherically averaged temperature difference of only 2K between summer and winter, compared to 34K in the NH (table S1).

The globally averaged annual mean rainfall in the NorthlandBright simulation is approximately 2 mm/day. Unsurprisingly, more of this rain falls over the ocean (2.9 mm/day) than over the continent (1.5 mm/day), with a strong latitudinal dependence (figure 2b). The ITCZ has a strong seasonal cycle, with heavier rainfall and a peak that extends farther polewards over the ocean than over the continent (figure 2b, 3a). Over the continent, the ITCZ reaches its farthest northwards extent during August and September, with the peak in precipitation reaching approximately 15°N. In contrast, the peak in the ITCZ over the ocean occurs at around 20°S during March, with roughly double the rate of precipitation in the ocean ITCZ-peak than the land ITCZ-peak. The land cannot support as strong an ITCZ because all the moisture for the ITCZ must initially be brought onto the land each season by ITCZ precipitation; in contrast, the ocean provides an unlimited supply of water in the form of nearby evaporation that can subsequently be precipitated in the SH ITCZ.

In NorthlandBright, moist air is transported from the ocean onto the continent, where it rains out in the tropics. Terrestrial tropical precipitation is most intense from August to November. The land water evaporates quickly in the tropics due to high insolation (i.e. evaporation has a similar seasonal cycle to precipitation; figure 3a-c). North of 20°N, precipitation is roughly equal

to evaporation in the annual mean (not shown). Despite heavy wet-season precipitation in the tropics, the ground between 0-20°N dries out during the dry season (February-June), because of strong seasonal evaporation (figure 3b,d).

In the subtropics of the Northern Hemisphere (roughly 20-40°N) there is a desert with dry soil year-round (figures 2b, 3d). Extratropical precipitation in the land hemisphere features a broad maximum in NH summer that extends from 50°N to the pole that is likely due to localized convection (figure 2b). In the ocean hemisphere, the extratropical maximum in precipitation is located at about 40°S, and is storm track precipitation associated with baroclinic cyclones (figure 2b). Precipitation in the ocean hemisphere storm track is nearly seasonally invariant.

The high latitude soil is saturated or nearly saturated with water year-round, forming what we call the "Great Northern Swamp" (figure 3d), with slightly less terrestrial water storage during June-July when evaporation (fueled by increased summer insolation) exceeds precipitation (figure 3c-d). Interestingly, the soil moisture in the Great Northern Swamp is supplied by water transport from the tropics, and not from local moisture recycling alone. This becomes clear when the land is initialized without any water (NorthlandEmpty). In this simulation, the high latitude soil water is indistinguishable from NorthlandBright within 4-5 years (figures 3d-e). The transport of water to the poles is explored further in section e.

b. Climate impacts of land albedo

As we would expect, reducing the albedo of the land surface (making the land darker) leads to surface warming. In NorthlandDark, the land albedo is the same as that of the ocean. As such, the land hemisphere absorbs more solar energy in NorthlandDark than in NorthlandBright (figure S2b), leading to greater temperatures year-round (figure 2c). The additional shortwave (SW) radiation absorbed in NorthlandDark compared to NorthlandBright is released to the atmosphere in

the form of longwave (LW) radiation, sensible heat or latent heat (figure S2c-f). Increased temperatures and increased water vapor (resulting in similar relative humidity over the continent between NorthlandDark and NorthlandBright, figure 2e) lead to more downwelling longwave radiation at the surface (figure S2a). That is, the warming in NorthlandDark is not only due to increased SW absorption, but also due to increased downwelling LW at the surface. NorthlandDark is warmer than NorthlandBright over both land (+7.4K, figure 2c, table S1) and ocean (+2.4K, figure 2c, table S1), due to atmospheric transport of water vapour and heat. The continent in NorthlandDark is not only warmer than NorthlandBright - it is also wetter, particularly during the months of August-October, when the ITCZ shifts north (figure 2d).

c. Climate impacts of reduced terrestrial evaporation

NorthlandDry is the same world as NorthlandBright, except evaporation from the land surface is suppressed. With all else held equal (i.e. the same amount of incoming energy to the land surface, the same water availability, etc.), this reduction in evaporation from the land surface is expected to lead to greater surface temperatures. This is because if evaporative cooling is reduced, the energy absorbed by the surface must be emitted in the form of sensible heat or longwave radiation, both of which require an increase in surface temperatures. Indeed, both Shukla and Mintz (1982) and Laguë et al. (2019) find that reducing evaporation from the land surface leads to surface warming over land.

Contrary to previous literature, we find that suppressing evaporation over Northland leads to cooler, not warmer, surface temperatures. Annual mean temperatures in NorthlandDry are 3.2K cooler globally, and 4.9K cooler over land than NorthlandBright (figure 2c, table S1). The cold anomaly is fairly homogeneous over the ocean hemisphere, but is at its greatest during JJA in the northern subtropics (figure 2c). This is surprising as the latent heat flux over land is greatly

reduced in NorthlandDry compared to NorthlandBright (figure 5e), which we would expect to lead to warming. However, suppressing terrestrial evaporation also reduces the amount of water vapour released to the atmosphere over terrestrial regions. Water vapour is a strong greenhouse gas, and if atmospheric water vapour is depleted in sufficiently large quantities, the reduction in the amount of longwave radiation absorbed by the atmosphere and re-emitted down towards the surface would lead to net cooling. Moreover, while the direct warming effect of reducing latent cooling is locally isolated to the region where evaporation is reduced, the cooling associated with reduced atmospheric water vapour is much broader in spatial extent, as the atmosphere can mix water vapour (or air with reduced water vapour) beyond the locations where terrestrial evaporation was reduced.

The decrease in atmospheric water vapor (figure 2f) due to reduced evaporation from the land surface cools NorthlandDry relative to NorthlandBright by reducing downwelling longwave radiation (figure 5a). This reduction in downwelling longwave radiation greatly exceeds the reduction in latent heat flux (which on its own would lead to warming). The reduction in downwelling longwave radiation reaches 150 W/m^2 in the northern high latitudes, while the reduction in latent heat flux peaks at around 80 W/m^2, with the largest reductions in the northern tropics and high latitudes (compare figure 5a with 5e). In the dry subtropics, the latent heat flux is already near-zero for most of the year in NorthlandBright, so suppressing evaporation has little impact on temperature in this region (figure 5e). Hence, cooling is strongest in the dry subtropics, particularly during JJA (figure 2c), because the cooling due to the reduction in downwelling longwave from reduced atmospheric water vapor has no warming offset from local reductions in latent cooling. There is actually a slight increase in net shortwave radiation absorption at the surface over land during NH summer months due to reduced absorption of shortwave radiation by water vapor (figure 5b). However, the

decrease in the downwards emission of longwave radiation from reduced atmospheric water vapor dominates the change in absorbed surface energy (figure 5f).

At the TOA, there is a substantial reduction in net energy absorbed over the continent from June-August, and an increase in net energy absorbed at the TOA over the continent from September-December (figure 6c). These changes are dominated by the change in TOA LW. During NH summer, more LW is lost from the TOA as a result of a smaller greenhouse effect, and there is less net SW absorption due to reduced atmospheric water vapor (figure 6). That is, despite the surface being colder during JJA in NorthlandDry than NorthlandBright, there is still more LW lost from the TOA in NorthlandDry because of the reduced greenhouse effect. This contrasts with the driver of changes in TOA LW from September-December, when there is overall more energy absorbed at the TOA in NorthlandDry than NorthlandBright (figure 6c). In this case, NorthlandDry has less LW emission from the TOA, reflecting the overall colder conditions in NorthlandDry compared to NorthlandBright (figure 6b).

We can compare the change in land surface temperature over Northland due to suppressed terrestrial evaporation to an equivalent change in albedo, if we assume land surface temperatures scale linearly with land surface albedo (as suggested holds in Laguë et al. (2019)). The surface temperature change between NorthlandDark and NorthlandBright implies a 9.9K increase in land surface temperatures per 0.1 decrease in land surface albedo for our idealized planet (see table S1). We note that this is much larger than the roughly 2K increase in surface temperatures per 0.1 decrease in land surface albedo found in Laguë et al. (2019), for a realistic continental configuration in a more complex model. However, intuitively this value should vary with total land area, land distribution, and cloud cover (which is not represented in this model), as modifying land albedo will have a different impact on absorbed SW energy and surface temperatures depending on the presence of clouds, incident solar radiation, and surface moisture in the location of the albedo

change. Applying the 9.9K/0.1 decrease in albedo relationship for Northland to the temperature change in NorthlandDry vs. NorthlandBright tells us that suppressing terrestrial evaporation over Northland has the equivalent effect on land surface temperatures as increasing the NH albedo by 0.05 (roughly 14%, 0.05/0.35).

The response of precipitation to suppressed terrestrial evaporation in the NorthlandDry experiment is widespread. In particular, precipitation over the continent decreases almost to zero during August-October, which is the wettest part of the year in NorthlandBright. A very weak ITCZ generates a small amount of precipitation over the southern edge of the continent in August-October (figure 2d), while precipitation is very low over the rest of the continent year round. We note that the structure of the Hadley cell during JJA in NorthlandDry differs from the Hadley cell of the other simulations presented here (figure S3). NorthlandDry does not have a large source of moisture over the land surface in the tropics. The ITCZ is very weak during JJA (figure 4c), and rather than an overturning circulation driven by the release of latent heat, the circulation is driven by direct thermal heating of the surface. The result is two overturning cells stacked on the equator during JJA, with the lower cell circulating anti-clockwise and the upper cell circulating clockwise (figure S3f).

d. Temperature response to suppressed evaporation in various continental configurations

The unexpected cooling of Northland with suppressed terrestrial evaporation is due to the reduction in downwards LW from reduced atmospheric water vapor (and thus a weaker greenhouse effect) dominating any surface warming from reduced latent heat fluxes. Because the Northland continental configuration has no oceanic water source in the NH, NH atmospheric water vapor becomes significantly depleted (figure 8o). We further explore the effects of suppressing terrestrial evaporation on surface temperature by considering four additional continental configurations with

varying amounts of ocean in the NH: ThreeQuarterLand, NorthWestLand, ThreePatchLand, and TwoPatchLand (figure 1, table 1). We compare simulations where the continents have the same land surface properties as NorthlandBright (i.e. "normal" land surface properties) to simulations where the continents have the same land surface properties as NorthlandDry (i.e. terrestrial evaporation is suppressed), to explore the trade-off between warming from reduced surface latent heat flux and cooling from reduced atmospheric water vapor.

In TwoPatchLand, suppressing terrestrial evaporation leads to 1.0K of warming over land, on average (figure 7a). However, as with the dry regions of NorthlandBright, suppressing evaporation over regions that are climatologically dry in TwoPatchLand (i.e. the subtropics) does not lead to any direct warming through reduced evaporative cooling (figure 8a). Instead, these subtropical land areas experience cooling when terrestrial evaporation is suppressed as a result of decreased downwards LW from reduced atmospheric water vapour. In NorthWestLand, suppressing evaporation also generally leads to warming over land, with an average warming of 0.7K over land (figures 8b, 7). The warming is not as strong in NorthWestLand as in TwoPatchLand when evaporation is suppressed, despite both continental configurations having the same total land area and the same latitudinal distribution of land area, with 1/2 of the NH covered by land. The warming is smaller in NorthWestLand despite a comparable (indeed, slightly smaller) reduction in terrestrial latent heat flux (figure 7b).

ThreePatchLand and ThreeQuarterLand have the same total land area and in both cases 3/4 of the NH are covered by land. However, suppressing terrestrial evaporation leads to warming of the land for ThreePatchLand, and cooling of the land for ThreeQuarterLand (figure 7a). The warming of 0.3K over land in ThreePatchLand is smaller than in TwoPatchLand or NorthWestLand, reflecting the larger reduction in atmospheric water vapor (figure 8f) driven by more land area. In ThreeQuarterLand, the reduction in atmospheric water vapour is large enough to dominate warming

from reduced latent heat flux, resulting in net land cooling of 0.3K (figures 7a, 8j,l). The reduction in latent heat flux from land is larger in ThreePatchLand than ThreeQuarterLand, but the reduction in latent heat flux from the ocean is much larger in ThreeQuarterLand than in ThreePatchLand (figure 7b). The differences between ThreePatchLand and ThreeQuarterLand (and TwoPatchLand and NorthWestLand) demonstrate that it is not only land area, but also continent size and distribution that modulates the temperature response to suppressed terrestrial evaporation.

The change in terrestrial latent heat flux due to suppressed evaporation over land (figure 7b) is approximately equal to the latent heat flux from the simulations with "normal" surface properties (from NorthlandBright), because there is almost no evaporation in the simulations with NorthlandDry land surface properties. The single large continents have slightly lower latent heat fluxes in the "normal" simulations than their patchy counterparts; that is, TwoPatchLand and ThreePatchLand have slightly larger terrestrial latent heat fluxes than NorthWestLand and ThreeQuarterLand, respectively, and thus have slightly larger changes in latent heat flux from land when terrestrial evaporation is suppressed.

However, we note that the average area-weighted change in latent heat flux from the land surface is of comparable magnitude across all the continental configurations considered here (figure 7b), while total reduction in terrestrial latent heat flux scales with total land area. For simulations with the same total land area (e.g. TwoPatchLand and NorthWestLand), the total reduction in terrestrial latent heat flux is similar, but the surface temperature response differs. The temperature change driven by suppressing terrestrial evaporation is greater when the contiguous continental area is larger. This occurs because the atmosphere becomes more depleted in water vapor over a single large continent than it does over two smaller continents separated by ocean. Thus the water vapor cooling effect is stronger over larger continents than smaller ones, even if the direct warming due to reduced latent cooling of the surface is similar.

Over the oceans, surface temperatures cool and evaporation is reduced as a result of suppressing terrestrial evaporation in all the TwoPatchLand, ThreePatchLand, NorthWestLand, ThreeQuarterLand, and Northland continental configurations (figure 8). The changes in latent heat flux from the ocean (blue bars in figure 7b) must be the result of changes in the local oceanic surface energy budget. For example, cooling over the NH ocean in ThreeQuarterLand is more intense than it is over the NH ocean in ThreePatchLand (figure 8 g vs j), which is consistent with a greater reduction in oceanic latent heat flux in ThreeQuarterLand vs. ThreePatchLand. Despite Northland showing the greatest surface cooling and the greatest global reduction in latent heat flux, the reduction in oceanic latent heat flux in Northland is small compared to the other continental configurations (figure 7b). This reflects the fact that most of the temperature change in Northland occurs over the land hemisphere, and not over the ocean. In the other continental configurations, much of the reduction in oceanic latent heat flux occurs over the NH, where the temperature changes and decreases in atmospheric water vapour are greatest (figure 8). The cooling over the ocean is due to a reduction in atmospheric water vapor from suppressed terrestrial evaporation leading to reductions in downward LW. In turn, cooling over the ocean reduces evaporation from the ocean due to the Claussius Clapeyron relationship. This generates a weak negative feedback on the ocean temperature but also further reduces water vapor flux to the atmosphere. Only in a few ocean regions do we see a slight increase in evaporation (not shown), as might be expected if drier air was being advected off the continent. However, these regions are not all located downstream of the continents; most of the ocean shows a decrease in evaporation due to a reduced greenhouse effect.

We can also consider differences between NorthlandDark and Aqua, as the NH in NorthlandDark has the same albedo as Aqua but a limited capacity to hold water. On the one hand, one might expect the NH land surface in NorthlandDark to be warmer than in Aqua because of limited water available for evaporation (thus potentially less latent cooling of the surface). On the other

hand, reduced atmospheric water vapor in the NH of NorthlandDark compared to Aqua could result in cooling (due to a weaker greenhouse effect). In the comparison of NorthlandDark to Aqua however, we are not simply considering differences in water availability; the different NH heat capacities in NorthlandDark and Aqua also leads to differences in evaporation and surface temperatures. The smaller heat capacity over the land surface in NorthlandDark results in a much larger seasonal cycle in surface temperatures, with hotter summers and cooler winters (figure 9d). The difference in heat capacity also generates big differences in NH evaporation between NorthlandDark and Aqua, since the available energy at the surface in NorthlandDark is used not only to heat the surface, but also to evaporate water (figure 9b,e). In NH summer, high surface temperatures cause a high vapor pressure deficit. Combined with the low heat capacity that requires more energy to be lost by the land surface as heat or moisture, this drives larger latent heat fluxes from the high latitude land in NorthlandDark than in Aqua, despite Aqua having effectively unlimited water to evaporate. In the annual mean, the tropics in NorthlandDark are hotter and have lower latent heat fluxes than Aqua, while in the high latitudes, surface temperatures are lower and evaporative fluxes are higher. This results in an atmosphere that is drier over the NH in the low latitudes, but actually less dry over the NH high latitudes in NorthlandDark than Aqua (figure 9c). This is notably different from the TwoPatchLand, ThreePatchLand, NorthWestLand, and ThreeQuarterLand simulations, but is driven primarily by differences in the heat capacity of land vs. ocean, rather than differences in water availability/evaporation.

In summary, we find that suppressing terrestrial evaporation has a direct local warming effect on the region of evaporative suppression, by reducing latent cooling of the land surface. However, suppressing terrestrial evaporation indirectly cools globally by reducing atmospheric water vapour (a strong greenhouse gas). In the case of TwoPatchLand, NorthWestLand, and ThreePatchLand, the local warming effect dominates the response in most terrestrial regions, while the dominant

effect over ocean and desert land regions is cooling associated with decreased atmospheric water vapour (figure 7a). However, when evaporation is suppressed over ThreeQuarterLand and Northland, the atmospheric water vapour effect dominates resulting in cooler surface temperatures everywhere (figure 7a). Because Northland does not have any ocean in the Northern Hemisphere, the atmosphere can become much more depleted in water vapour than occurs in the other continental configurations (figure 8o). In TwoPatchLand, NorthWestLand, and ThreePatchLand, atmospheric water vapor is depleted over the continents, but is replenished over the ocean at all latitudes, such that the zonal-mean reduction in atmospheric water vapor is much less than the water vapor reduction in Northland (figure 8, right column). While the reduction in atmospheric water vapour isn't as large in ThreeQuarterLand as in Northland, it is large enough for the mean response of land temperatures to be an overall cooling (figures 7a, 8j). We deduce that the land surface temperature response to reduced terrestrial evaporation is a function of both total land area (which controls the reduction in terrestrial latent heat flux) and contiguous continent size (which controls how dry the atmosphere becomes).

e. The role of moisture transport

In all the Northland simulations except NorthlandDry (which can't store water on land), a Great Northern Swamp forms in the northern high latitudes. In the absence of a large low-latitude water source, is the Great Northern Swamp sustainable? Here we use an all-land simulation, Lakeworld, to show that the existence of the Great Northern Swamp relies on atmospheric moisture transport from the SH ocean in all other Northland experiments. Lakeworld has no ocean; land surface properties are similar to those in NorthlandBright except that lakes of arbitrary depth are allowed to form on all gridcells, if precipitation exceeds evaporation.

Lakeworld rapidly forms two lakes, one over each pole (figure 3f), which deepen as the simulation progresses. Within a few years, all of the water on Lakeworld - which is initialized with 100mm of water in every gridcell - has been transported to the polar high latitudes, and the land in the tropics is completely dry year-round. The lake edges retreat polewards quickly over the first 35 years, then more slowly as the simulation progresses.

In effect atmospheric circulation redistributes water to concentrate it in the polar regions. On the present-day Earth, the lower branch of the Hadley circulation transports moisture equatorward, but in Lakeworld the moisture is rapidly mixed poleward by mid-latitude eddies, then trapped too far poleward for this mechanism of equatorward transport. The atmosphere of Lakeworld is very dry, with atmospheric moisture isolated to the lower troposphere near the summer pole (figure S4). Because the atmosphere in Lakeworld is so dry, the greenhouse effect is very weak, causing Lakeworld to be much colder than the simulations that include some ocean (figure S1, S5). Surface temperatures in Lakeworld are above the freezing point year round in the lower latitudes, and at higher latitudes during summer (figure S5).

The polar lake in Lakeworld has a much smaller latitudinal extent than the Great Northern Swamp in the Northland simulations. The southern portion of the Great Northern Swamp in Northland receives moisture transport from mid-latitude eddies, which does not occur in Lakeworld, where the moisture is trapped at the poles after the first few years of the simulation. The lake continues to drift poleward over the course of the Lakeworld simulation. The Lakeworld simulation would have to be run to equilibrium to determine how far poleward the polar lake will retreat. However, we do not continue the Lakeworld simulation beyond 80 years as (a) the extent of the polar lake in equilibrium is not the focus of this study and (b) the atmosphere in an all-land configuration leaks moisture in the current configuration of Isca (figure S6). We also explore an all-land simulation that cannot form lakes (i.e. it has the same land surface properties as

NorthlandBright). Like Lakeworld, that simulation also quickly transports water to the poles, but because runoff is discarded when soil moisture exceeds the bucket capacity, the simulation rapidly loses water from the system (not shown).

f. Land's influence on ITCZ location

Here we discuss the unique behavior of the ITCZ in the Northland continental configurations. We find that the ITCZ in *both* hemispheres of all Northland experiments extends farther poleward than in Aqua (with the exception of NorthlandDry, which has very little precipitation over land), despite the greater water vapour content and absorbed SW radiation in Aqua. There is an extensive literature exploring how hemispherically asymmetric sources of energy to the atmosphere cause the atmosphere to transport energy from the energy-rich hemisphere to the energy-poor hemisphere, with a corresponding shift in the zonally averaged ITCZ towards the energy-rich hemisphere (Kang et al. 2008; Yoshimori and Broccoli 2008; Fasullo and Trenberth 2008; Donohoe et al. 2013; Geen et al. 2020). The relationship between the magnitude of cross-equatorial energy transport and the location of the ITCZ has been explored for the modern Earth system, where the ITCZ shifts 2.4-2.7°S per PW increase in northward cross-equatorial energy transport (Donohoe et al. 2013). In our idealized simulations, we find a marginally steeper relationship than Donohoe et al. (2013), with a 3.4° southward shift in the annual mean ITCZ latitude per PW increase in northward cross-equatorial energy transport (figure 10, S7).

The greater poleward extent of the zonally averaged ITCZ location is best explained by comparing the NorthlandDark and Aqua experiments, since these two configurations have the same surface albedo and differ only in the heat capacity and capacity to store water in the NH. We argue that the primary reason for the greater poleward extent of the ITCZ in the Northland simulations is

the difference in heat capacity between the land and ocean hemispheres, which generates a larger hemispheric energy imbalance than in Aqua (both seasonally and in the annual mean).

The lower heat capacity of the NH in NorthlandDark provides less of a buffer to the atmospheric energy imbalance by storing less energy in the surface relative to Aqua during JJA, and releasing less energy during DJF (compare SFC in figure 11f,h and j,l). During JJA, the ITCZ extends farther poleward over the NH in NorthlandDark than Aqua, because the land surface takes up little energy, resulting in a larger atmospheric energy source F_{net} in NorthlandDark than Aqua (Geen et al. 2020). During DJF, the ITCZ extends farther poleward over the SH in NorthlandDark than Aqua because the land surface releases little energy, while in Aqua the ocean releases stored energy to the atmosphere; thus, the NH atmosphere is more energy-poor in NorthlandDark than Aqua during DJF. The net effect is that the NH atmospheric energy source is much larger in NorthlandDark than Aqua during JJA, while the NH atmospheric energy source is more negative during DJF in NorthlandDark than Aqua (compare F_{net} in figure 11f,h and j,l, table S2). In the annual mean, NorthlandDark has a hemispheric imbalance in F_{net}, while F_{net} is symmetric about the equator in Aqua (table S2). This hemispheric energy imbalance results in an annual mean transport of energy across the equator from the SH to the NH, consistent with a zonally averaged ITCZ sitting south of the equator (figure 10). Corresponding to this hemispheric atmospheric energy imbalance, the ITCZ in NorthlandDark extends much farther poleward than the ITCZ in Aqua, both seasonally and in the annual mean. In NorthlandBright and NorthlandDry, the ITCZ extends slightly further south than in NorthlandDark during DJF because the lower surface albedo (NorthlandBright) and lower water vapor (NorthlandDry) reduces the total amount of energy taken up during NH summer and subsequently released in NH winter by the land surface, accentuating the hemispheric imbalance in the atmospheric energy source that already exists as a result of the

smaller heat capacity of land vs. ocean (figure 11a,c; table S2). Details of the calculations used for figures 10 and 11 are provided in the supplement.

4. Discussion

a. Temperature response to suppressed terrestrial evaporation

With all else held equal, reducing evaporation from the land surface should lead to surface warming, as the energy formerly used to evaporate water is instead re-partitioned into sensible heat or emitted longwave radiation. While reducing evaporation from the land surface directly leads to warming (Shukla and Mintz 1982; Laguë et al. 2019), reducing water flux from the land surface also impacts atmospheric concentrations of water vapor, a strong greenhouse gas. Given the competing effects of reduced evaporative cooling which would lead to warming, and reduced longwave trapping by atmospheric water vapor which would lead to cooling, we hypothesize that a crossing-point exists in the temperature response to suppressed land evaporation (figure 12). Starting from a state of sufficient atmospheric moisture, reducing evaporation from the land surface should initially lead to surface warming as a result of decreased evaporative cooling of the land surface ((i) in figure 12). However, as atmospheric water vapor concentration decreases, the strength of the atmospheric greenhouse effect also decreases, inducing a cooling effect on the surface; the warming signal from suppressed evaporation competes with the cooling from a reduced greenhouse effect ((ii) in figure 12). Once atmospheric concentrations of water vapor are sufficiently low, the cooling effect from the reduced atmospheric greenhouse effect dominates the surface temperature response ((iii) in figure 12).

From our simulations, suppressing evaporation over TwoPatchLand would fit into regime (i), where reduced evaporation warms the land surface. NorthWestLand falls between regimes (i) and

(ii), where the direct warming effect of reduced evaporation is weaker than in TwoPatchLand, thus the total warming is more strongly damped by the reduction in atmospheric water vapour. ThreePatchLand and ThreeQuarterLand bracket the crossing-point of the temperature response (regime ii), with ThreePatchLand warming slightly and ThreeQuarterLand cooling slightly. Northland falls firmly into regime (iii), where any direct warming of the surface is more than out-weighed by cooling from reduced atmospheric water vapor. Generally, larger total land areas fall further to the right on this curve; however, for the same total land area (e.g. TwoPatchLand vs. NorthWestLand), the continental arrangement with the larger contiguous continent size falls further to the right. This occurs because when the continents are broken up, the atmosphere can be replenished with water vapor when it passes over the ocean, while in the case of a larger contiguous continent, the atmosphere becomes more depleted in water vapor. We suggest the present-day continental configuration of Earth falls into regime (i), both because the present-day continental configuration of Earth most closely resembles TwoPatchLand (i.e. there is ample ocean at every latitude), and because previous modeling studies (e.g. Shukla and Mintz 1982; Laguë et al. 2019) find that reducing terrestrial evaporation leads to surface warming.

In our simulations, suppressing terrestrial evaporation in all of our continental configurations leads to cooling over the ocean. This differs from the results of Shukla and Mintz (1982) and Laguë et al. (2019), who found that reduced evaporation with a realistic present-day continental configuration leads to surface warming not only over the land, but also over parts of the ocean. The continental configuration could be one reason for the difference in our results; in the present-day continental configuration, there is a large area of ocean at every latitude. Thus, even if terrestrial evaporation were completely suppressed, dry continental air could advect over the ocean and gain water vapour. However, this is also the case for TwoPatchLand and ThreePatchLand, where we find the land warms but the ocean cools in response to suppressed terrestrial evaporation. An-

other reason to expect differences in the temperature response to reduced terrestrial evaporation in this study vs. previous studies relates to model complexity; both the GLAS (Shukla and Mintz 1982) and CESM (Laguë et al. 2019) models which showed oceanic warming include the effects of cloud cover. We suspect the difference in the response of ocean temperatures to suppressed terrestrial evaporation between this study and those of Shukla and Mintz (1982) and Laguë et al. (2019) is driven by model differences. In particular, our idealized Isca simulations do not have any representation of cloud cover, and cloud responses to changes in terrestrial evaporation can have large climate feedbacks (Laguë et al. 2019). Understanding how the presence of clouds, and the response of clouds to reduced terrestrial evaporation, modify the temperature response to reduced terrestrial evaporation both on land and globally requires future study.

Based on our results from TwoPatchLand/ThreePatchLand versus NorthWestLand/ThreeQuarterLand (section d), we postulate that suppressing terrestrial evaporation in continental configurations with large amounts of arid land (e.g. polar continents) would have a much weaker impact on water vapour than continents with moist climates (e.g. in the tropics), and thus would not generate strong large-scale cooling. We note that we have tested an extreme level of reduced terrestrial evaporation here. We do not consider the response of temperature to smaller reductions in terrestrial evaporation such as those driven by the closure of plants' stomata in response to increased atmospheric CO_2, which have been shown to generate terrestrial warming across CMIP 5 and 6 models (Zarakas et al. 2020).

We have explored the temperature response to suppressing terrestrial evaporation over idealized NH continents; in doing so, we have demonstrated that continental configuration is of utmost importance in controlling the temperature response to suppressed terrestrial evaporation. We have identified the competing effects of suppressing terrestrial evaporation on surface temperature without any complicating factors driven by cloud responses. These idealized simulations do not

represent cloud cover, thus do not capture either how the presence of clouds may modulate the surface temperature response to reduced terrestrial evaporation, or how cloud changes in response to reduced terrestrial evaporation may further influence surface temperatures, both locally over land and over the ocean. Further study is required to identify the seasonality of this response, which continental configurations lead to warming vs. cooling, what level of reduction in continental evaporation is required for warming vs. cooling, and what role clouds play in modulating the temperature response to reduced terrestrial evaporation. Additional study is also needed to determine where and how much this response may matter on the present-day Earth.

b. Connections to Snowball Earth

Our results raise the question of how past continental configurations and distributions of water and vegetation on those continents may have impacted both terrestrial and global paleoclimate through water vapor feedbacks. What is the distribution of continents that is required such that decreasing evapotranspiration from the land surface leads to a cooling rather than warming? In present-day Earth, the greenhouse effect is due mainly to water vapor, and the source of water vapor is net evaporation in the tropics (equatorward of 35° latitude) which is distributed globally by atmospheric circulation. In our TwoPatchLand and NorthWestLand continental configurations, suppressing terrestrial evaporation results in global-scale cooling through reduced atmospheric water vapour, though the land surface generally warms due to reduced latent cooling. However, in our Northland continental configuration, the continent covers the entire hemisphere, which severely reduces the evapotranspiration of water vapor poleward of the ITCZ in the NH. Further reducing terrestrial evaporation in the NorthlandDry experiment reduces the greenhouse effect and causes cooling. In this regard, it is illuminating to consider the Snowball Earth events: global glaciations during which ice covered the entire surface of the Earth (Kirschvink 1992; Hoffman

et al. 2017). There is evidence for two such events during the Neoproterozoic (between 630 and 750 million years ago) and one in the early Paleoproterozoic (2.5 billion years ago) (Abbot et al. 2013; Hoffman et al. 2017), when most of the continental land masses were located in the tropics (see Kump et al. 2004; Worsley and Kidder 1991, and references therein).

The Snowball Earth atmosphere is cold and holds little moisture (Voigt et al. 2011; Hoffman et al. 2017). Past work suggests that paleogeographic continental configurations cause a reduction in atmospheric water vapor compared to an aquaplanet without continents, increasing direct heating by decreasing cloud cover (Fiorella and Poulsen 2013). Future work could test the robustness of this result and probe whether past tropical megacontinents were large enough to cause a sufficient reduction in tropical water vapor to cool the tropics and contribute to the onset of Snowball events (though the dry atmosphere of Snowball Earth is attributed to the cold temperatures and not vice versa (Voigt et al. 2012; Hoffman et al. 2017)). This reduction in tropical water vapor would cause even greater cooling in the extratropics as a consequence of reduced atmospheric energy transport (Rose et al. 2014). If this occurred, cooling by reduced terrestrial evapotranspiration would help explain why Snowball Earth happened. However, reductions in continental precipitation would reduce the rate of silicate weathering, thus allowing for greater CO_2 buildup in the atmosphere, which would act against the formation of a Snowball Earth event. In addition, past tropical supercontinent configurations would have had some ocean at each latitude band, thus may more closely resemble our NorthWestLand or ThreeQuarterLand simulations than our Northland simulations. Notably, the NorthWestLand and ThreeQuarterLand configurations bracket the transition from warming to cooling when land evaporation is suppressed, suggesting this process could be relevant for Pangea-like continental configurations, though we have not explored the effect of varying the position (e.g. moving the whole continent to the tropics) of the megacontinent here.

We note that our NorthlandDry simulation has a similar JJA Hadley cell structure as Snowball Earth. The lack of moisture on the land surface in NorthlandDry means that over the continent during NH summer, as in Snowball Earth, the Hadley circulation is dominated by dry dynamics and produces a much smaller overturning circulation than in the present climate (Voigt et al. 2012; Voigt 2013).

c. Precipitation

In our Northland simulations, we find that the polewards extent of the ITCZ over the ocean hemisphere is influenced by the existence of the NH continent. Specifically, we find the small heat capacity and lower water vapor concentrations of the NH lead to the ocean hemisphere ITCZ extending much farther polewards than it does in an aquaplanet simulation. This is similar to the findings of Bordoni and Schneider (2008) and Wei and Bordoni (2018), that ITCZs in aquaplanets with shallower slab oceans extend farther polewards due to stronger energy gradients between the summer and winter hemispheres. Our Northland simulations also demonstrate the importance of hemispheric asymmetries in surface heat storage.

Previous studies have shown how hemispheric energy imbalances drive shifts in the zonal mean location of the ITCZ (e.g. Chiang and Bitz 2005; Broccoli et al. 2006; Kang et al. 2008; Swann et al. 2012; Maroon et al. 2016). In the current continental configuration on Earth, zonal mean changes are not generally representative of regional precipitation change (Byrne and O'Gorman 2015; Kooperman et al. 2018; Atwood et al. 2020). However, given our zonally symmetric continental distribution in Northland, the energy balance framework is a useful tool for understanding the seasonal cycle of circulation and the distribution of precipitation.

In Earth's present day continental configuration, roughly 68% of the total land mass is in the NH while the remaining 32% is in the SH. This work raises the question of how much the present

day continental configuration impacts the ITCZ location via asymmetries in seasonal heat storage between the hemispheres.

The present study ties into previous work exploring the impact of continental land masses on the climate system. The tropical rain belts with an annual cycle and a continent model intercomparison project (TRACMIP, Voigt et al. 2016) showed that the presence of an idealised tropical continent spanning 45° in longitude generally leads to a decrease in global-mean surface temperatures compared to an aquaplanet in several different GCMs. The authors noted that while this cooling might be expected from the increase in planetary albedo, the patterns of change are more complex and probably related to changes in cloud cover. Voigt et al. (2016) used a "jello-continent", which is essentially a patch of thin (lower heat capacity) ocean with higher albedo and reduced evaporation. In contrast to our study, there is no limit on water availability for evaporation over the jello-continent, which would be equivalent to unlimited soil moisture in our experiments. Simulations with "jello" continents in an Earth-like configuration generally capture the present-day climate well (Geen et al. 2018; Thomson and Vallis 2019), but might be too idealized for studying precipitation change in response to CO_2 forcing in some tropical regions such as the Amazon basin (Pietschnig et al. 2019). While the reduction in evaporation due to the presence of land leads to cooling in TRACMIP, similar to what we see from Aqua to NorthlandDark or from NorthlandBright to NorthlandDry, the mechanisms for the cooling are different. Firstly, clouds are not modelled in Isca but are noted to have an impact of surface temperature patterns in TRACMIP. Secondly, the inability of the jello-continent to dry out makes the "warming due to reduced latent cooling" (figure 12 (i)) less extreme, though at the same time the reduction in atmospheric water vapour – which would lead to cooling (figure 12 (iii)) – would be expected to be less drastic than in our study.

d. Relationship to all-land planets

Our Lakeworld simulation rapidly transports all the surface water to the poles. We expect this is because the climatological equator-to-pole temperature gradient ensures an even greater gradient in moisture (via the Clausius-Clapeyron relationship), and atmospheric storms transport water vapor towards the high latitudes where the vapor condenses and precipitates. The condensate remains at the poles because evaporation is greatly reduced by the cooling resulting from the reduced greenhouse effect. During summer, some of the high-latitude soil moisture evaporates, but is locally recycled. In the absence of an efficient mechanism to transport moisture from the poles towards the equator, all the moisture ends up accumulating in the polar regions. This "leaking" of moisture from the tropics to the poles warrants further study: e.g. how much water does the system require to maintain a moist tropics? What controls the latitudinal extent of the polar lake? This distribution of surface water is similar to that on other planets, such as Mars, which has two polar ice caps (Boynton et al. 2002; Wordsworth 2016; Feldman et al. 2004). While the mechanism by which the water on Mars is concentrated in its polar regions is unclear (Wordsworth 2016), we note that this is an intriguing similarity with our all-land simulation.

The presence of large topographical features could potentially modify the distribution of water on a land planet, as it could favour the formation of lakes via runoff into basins rather than at the poles, where the distribution of the lakes would be controlled by surface topography rather than atmospheric moisture transport alone, as is the case in our simulations. Indeed, previous studies of all-land planets that include overland river-like mechanisms to bring water back from the high latitudes to the low latitudes have high soil moisture outside of the polar regions and precipitation maxima in the mid latitude storm tracks (e.g. Kalidindi et al. 2018), unlike our Lakeworld simulation which has soil moisture maxima at the poles. In their land-planet simulation, Kalidindi et al.

(2018) find two distinct climate states in the absence of a seasonal cycle – one hot and dry, and one cold and wet. Including a seasonal cycle only produces a cold and wet state; while our all-land simulation is cold and wet near the poles, the absence of surface water redistribution means that the tropics in our Lakeworld simulation are cold (compared to Aqua or Northland) and dry. Differences between our results and those of Kalidindi et al. (2018) arise from the addition of clouds, zero obliquity, and importantly the resupply of water to low latitudes in their study. We suspect that without the water recycling mechanism and with a seasonal cycle, Kalidindi et al. (2018) would also observe low values of soil moisture and precipitation except very close to the poles.

e. Limitations

Certain caveats and limitations are inherent in our idealized framework. In this simplified GCM, there are no feedbacks associated with clouds. While cloud responses to terrestrial forcings have been identified in several studies (Hohenegger et al. 2009; de Arellano et al. 2012; Laguë and Swann 2016; Cho et al. 2018; Laguë et al. 2019; Kim et al. 2020), cloud responses are also a large source of uncertainty (Stocker et al. 2013; Zelinka et al. 2017). Redistribution of water within the land surface (e.g. due to rivers or topography) could significantly modify our soil moisture distribution (Kalidindi et al. 2018). We have also ignored surface albedo feedbacks associated with changes in snow or ice; while our simulations can drop below freezing, that has no effect on the surface albedo. We would expect the addition of an albedo feedback to amplify cooling when temperatures drop below freezing.

5. Conclusions

In this study, we use an idealized climate model to study the climate of Northland, a planet with a continent covering the NH and an ocean covering the SH, and several related continental

configurations where the NH contains both land and ocean. The physical properties of the land surface differ from the ocean in several ways, each of which has an effect on the climate system. Land has a limited capacity to hold water, a higher albedo, and a smaller heat capacity than oceans, and evaporation and turbulent energy exchange from the land surface is influenced by properties of vegetation and soils. By conducting a series of simulations where specific properties of the land surface are modified, we test the sensitivity of surface climate and atmospheric circulation to various aspects of the land surface.

The climatology of Northland has a seasonal temperature cycle that is greatly amplified over the land hemisphere, due to the limited heat capacity of the land surface. On the continent, the tropics are seasonally wet; moisture is brought onto the continent from the ocean by the land-falling ITCZ, but the soils dry out during NH winter. From 20°N-40°N, there is a desert region. In the high latitudes, soils are moist year round. There is rain over high latitude land during NH summer; in contrast, precipitation declines polewards of 45°S in the ocean hemisphere in all seasons. We show that atmospheric moisture transport forms a swampy region in the high latitudes, both in our Northland simulations and over a land-only planet.

Surprisingly, we find that suppressing terrestrial evaporation over the Northland continent leads to global-scale cooling, with particularly large cooling of 4.9K over the NH continent - this is in contrast to previous studies which find reducing terrestrial evaporation warms the land surface. With all else held equal, decreasing evaporation would lead to warming as the land surface would have to shed energy through sensible heat or emitted longwave radiation, both of which are a function of surface temperature. However, in our simulations, we find that suppressing terrestrial evaporation reduces atmospheric water vapor concentrations, and in turn decreases the strength of the greenhouse effect. The decrease in the greenhouse effect due to reduced water vapor leads to surface cooling which outweighs any surface warming resulting directly from reduced evaporative

cooling in the Northland continental configuration. Using a series of alternative continental configurations where only part of the NH is covered with land, we demonstrate that there is a trade-off between the local warming effect of reduced latent heat flux and the global cooling effect of reduced atmospheric water vapor. When the NH has two 90° wide continents separated by ocean, suppressing terrestrial evaporation leads to 1K of warming over land, while a single 180° wide NH continent leads to weaker warming of 0.7K over land. Three equally spaced 90° wide NH continents lead to even weaker warming of 0.3K over land, while a single 270° wide continent leads to cooling of 0.3K over land. The land only experiences warming as a result of suppressed terrestrial evaporation in regions with soil moisture. Suppressing terrestrial evaporation leads to reduced atmospheric water vapor and decreased downwelling LW over the oceans, which reduces ocean temperatures and evaporation from the oceans, in turn further reducing atmospheric water vapor. We conclude that both the terrestrial and global temperature response to suppressed terrestrial evaporation is not only a function of total land area or the latitudinal distribution of land, but also of continent size.

We find that the ITCZ extends much further polewards, both over the land and ocean hemispheres, in our Northland simulations compared to an aquaplanet simulation. This is primarily the result of the difference in surface heat capacity between the land and ocean hemispheres, which leads to a larger hemispheric imbalance in atmospheric energy in the Northland simulations compared to an aquaplanet.

By exploring the climate of Northland, this study provides insight into the role of hemispheric asymmetries in continental distribution on surface climate and atmospheric circulation, as well as into energetic constraints on the ITCZ location. We have identified a fundamental trade-off in the effect of terrestrial evaporation on surface temperatures which warrants further study. Northland provides an ideal limit for probing fundamental impacts of hemispheric asymmetries and raises

new questions about the role of continental distribution, planetary albedo, and terrestrial evaporation in modulating the climate system.

Data availability statement. The Isca climate model is publicly available at `https://github.com/ExeClim/Isca`. The data presented in this paper is archived on Dryad, accessible at `https://datadryad.org/stash/share/k1nIAE1nV4tfbZfbCQOp49qQp8xvlCyBoF9-c1jCDyU`. We will update this with a public link and doi (`https://doi.org/10.6078/D1399Q`) upon acceptance of this paper.

Acknowledgments. We wish to thank the organizers of the 2018 Advanced Climate Dynamics Course, where this project began (`https://www.uib.no/en/rs/acdc/118773/acdc-2018-hemispheric-asymmetry-climate`). We thank W. R. Boos, A. L. S. Swann, and W. Kang for their helpful discussions and feedback. We acknowledge postdoctoral funding support for MML from the James S. McDonnell Foundation. MP acknowledges funding by the University of Exeter College of Engineering Mathematics and Physical Sciences, and the UK - China Research and Innovation Partnership Fund through the Met Office Climate Science for Service Partnership (CSSP) China as part of the Newton Fund. In addition, MP's gratitude is due to the Rupert Ford Award (administered by the Royal Meteorological Society) and the University of Exeter College of Engineering Mathematics and Physical Sciences PhD Mobility Fund who provided the funding for her research visit to the University of Washington, Seattle, which facilitated collaboration on this project. We thank the editor and three reviewers for their thoughtful, constructive feedback on this manuscript.

References

Abbot, D. S., A. Voigt, D. Li, G. L. Hir, R. T. Pierrehumbert, M. Branson, D. Pollard, and D. D. B. Koll, 2013: Robust elements of snowball earth atmospheric circulation and oases for life. *Journal of Geophysical Research: Atmospheres*, **118 (12)**, 6017–6027.

Atwood, A. R., A. Donohoe, D. S. Battisti, X. Liu, and F. S. R. Pausata, 2020: Robust longitudinally-variable responses of the ITCZ to a myriad of climate forcings. *Geophysical Research Letters*, **47 (17)**, 1–13, doi:10.1029/2020GL088833.

Bonan, G. B., 2008: Ecological Climatology. Cambridge Univ. Press, Cambridge, UK.

Bordoni, S., and T. Schneider, 2008: Monsoons as eddy-mediated regime transitions of the tropical overturning circulation. *Nature Geoscience*, **1 (8)**, 515–519, doi:10.1038/ngeo248.

Boynton, W. V., and Coauthors, 2002: Distribution of hydrogen in the near surface of Mars: Evidence for subsurface ice deposits. *Science*, **297 (5578)**, 81–85, doi:10.1126/science.1073722.

Broccoli, A. J., K. a. Dahl, and R. J. Stouffer, 2006: Response of the ITCZ to Northern Hemisphere cooling. *Geophysical Research Letters*, **33 (1)**, 1–4, doi:10.1029/2005GL024546.

Budyko, M. I., 1961: The Heat Balance of the Earth's Surface. *Soviet Geography*, **2 (4)**, 3–13, doi:10.1080/00385417.1961.10770761.

Budyko, M. I., 1969: The effect of solar radiation variations on the climate of the Earth. *Tellus*, **21 (5)**, 611–619, doi:10.3402/tellusa.v21i5.10109.

Byrne, M. P., and P. A. O'Gorman, 2015: The response of precipitation minus evapotranspiration to climate warming: Why the "Wet-get-wetter, dry-get-drier" scaling does not hold over land. *Journal of Climate*, **28 (20)**, 8078–8092, doi:10.1175/JCLI-D-15-0369.1.

Canadell, A. J., R. B. Jackson, J. R. Ehleringer, H. A. Mooney, O. E. Sala, and E. Schulze, 1996: Maximum Rooting Depth of Vegetation Types at the Global Scale. *Oecologia*, **108 (4)**, 583–595.

Cess, R. D., and S. D. Goldenberg, 1981: The effect of ocean heat capacity upon global warming due to increasing atmospheric carbon dioxide. *Journal of Geophysical Research*, **86 (80)**, 498–502.

Charney, J. G., 1975: Dynamics of deserts and drought in the Sahel. *Quarterly Journal of the Royal Meteorological Society*, **101 (428)**, 193–202, doi:10.1002/qj.49710142802, URL http://dx.doi.org/10.1002/qj.49710142802%5Cnpapers2://publication/doi/10.1002/qj.49710142802.

Cheng, L., K. E. Trenberth, J. Fasullo, T. Boyer, J. Abraham, and J. Zhu, 2017: Improved estimates of ocean heat content from 1960 to 2015. *Science Advances*, **3 (3)**, e1601 545.

Chiang, J. C. H., and C. M. Bitz, 2005: Influence of high latitude ice cover on the marine Intertropical Convergence Zone. *Climate Dynamics*, **25 (5)**, 477–496, doi:10.1007/s00382-005-0040-5.

Cho, M. H., A. R. Yang, E. H. Baek, S. M. Kang, S. J. Jeong, J. Y. Kim, and B. M. Kim, 2018: Vegetation-cloud feedbacks to future vegetation changes in the Arctic regions. *Climate Dynamics*, **50 (9-10)**, 3745–3755, doi:10.1007/s00382-017-3840-5.

Croll, J., 1870: XII. On ocean-currents. *The London, Edinburgh, and Dublin Philosophical Magazine and Journal of Science*, **39 (259)**, 81–106.

Davin, E. L., N. de Noblet-Ducoudré, N. de Noblet-Ducoudre, and N. de Noblet-Ducoudré, 2010: Climatic Impact of Global-Scale Deforestation: Radiative versus Nonradiative Processes. *Journal of Climate*, **23 (1)**, 97–112, doi:10.1175/2009JCLI3102.1, URL http://journals.ametsoc.org/doi/abs/10.1175/2009JCLI3102.1.

de Arellano, J. V.-G., C. C. van Heerwaarden, and J. Lelieveld, 2012: Modelled suppression of boundary-layer clouds by plants in a CO2-rich atmosphere. *Nature Geoscience*, **5 (10)**, 701–704, doi:10.1038/ngeo1554, URL http://dx.doi.org/10.1038/ngeo1554.

Donohoe, A., K. C. Armour, G. H. Roe, D. S. Battisti, and L. Hahn, 2020: The Partitioning of Meridional Heat Transport from the Last Glacial Maximum to CO 2 Quadrupling in Coupled Climate Models . *Journal of Climate*, **33 (10)**, 4141–4165, doi:10.1175/jcli-d-19-0797.1.

Donohoe, A., and D. S. Battisti, 2011: Atmospheric and surface contributions to planetary albedo. *Journal of Climate*, **24 (16)**, 4402–4418, doi:10.1175/2011JCLI3946.1.

Donohoe, A., J. Marshall, D. Ferreira, and D. Mcgee, 2013: The relationship between ITCZ location and cross-equatorial atmospheric heat transport: From the seasonal cycle to the last glacial maximum. *Journal of Climate*, **26 (11)**, 3597–3618, doi:10.1175/JCLI-D-12-00467.1.

Eliassen, A., and E. Palm, 1960: On the Transfer of Energy in Stationary Mountain Waves. *Geofysiske Publikasjoner*.

Fasullo, J. T., and K. E. Trenberth, 2008: The Annual Cycle of the Energy Budget. Part II: Meridional Structures and Poleward Transports. *Journal of Climate*, **21 (10)**, 2313–2325, doi:10.1175/2007JCLI1936.1.

Feldman, W. C., and Coauthors, 2004: Global distribution of near-surface hydrogen on mars. *Journal of Geophysical Research: Planets*, **109 (E9)**.

Ferrari, R., and D. Ferreira, 2011: What processes drive the ocean heat transport? *Ocean Modelling*, **38 (3)**, 171–186, doi:10.1016/j.ocemod.2011.02.013, URL http://www.sciencedirect.com/science/article/pii/S1463500311000485.

Fiorella, R. P., and C. J. Poulsen, 2013: Dehumidification over tropical continents reduces climate sensitivity and inhibits snowball earth initiation. *Journal of Climate*, **26 (23)**, 9677–9695.

Forget, G., and D. Ferreira, 2019: Global ocean heat transport dominated by heat export from the tropical Pacific. *Nature Geoscience*, 1, doi:10.1038/s41561-019-0333-7, URL http://www.nature.com/articles/s41561-019-0333-7.

Geen, R., S. Bordoni, D. Battisti, and K. Hui, 2020: The Dynamics of the Global Monsoon - Connecting Theory and Observations. *Earth and Space Science Open Archive*, 1–26, doi:https://doi.org/10.1002/essoar.10502409.1.

Geen, R., F. H. Lambert, and G. K. Vallis, 2018: Regime Change Behavior during Asian Monsoon Onset. *Journal of Climate*, **31 (8)**, 3327–3348, doi: 10.1175/JCLI-D-17-0118.1.

Hartmann, D. L., 1994: *Global physical climatology*, Vol. 56. Academic press.

Held, I. M., 2005: The gap between simulation and understanding in climate modeling. *Bulletin of the American Meteorological Society*, **86 (11)**, 1609–1614.

Held, I. M., P. L. Panetta, and R. T. Pierrehumbert, 1985: Stationary external Rossby waves in vertical shear. 865–883 pp., doi:10.1175/1520-0469(1985)042⟨0865:SERWIV⟩2.0.CO;2.

Hoffman, P. F., and Coauthors, 2017: Snowball Earth climate dynamics and Cryogenian geology-geobiology. *Science Advances*, **3 (11)**, doi:10.1126/sciadv.1600983.

Hohenegger, C., P. Brockhaus, C. S. Bretherton, and C. Schär, 2009: The soil moisture-precipitation feedback in simulations with explicit and parameterized convection. *Journal of Climate*, **22 (19)**, 5003–5020, doi:10.1175/2009JCLI2604.1.

Jeevanjee, N., P. Hassanzadeh, S. Hill, and A. Sheshadri, 2017: A perspective on climate model hierarchies. *Journal of Advances in Modeling Earth Systems*, **9 (4)**, 1760–1771, doi:10.1002/2017MS001038.

Jin, Z., T. P. Charlock, W. L. Smith, and K. Rutledge, 2004: A parameterization of ocean surface albedo. *Geophysical Research Letters*, **31 (22)**, 1–4, doi:10.1029/2004GL021180.

Kalidindi, S., C. H. Reick, T. Raddatz, and M. Claussen, 2018: Two drastically different climate states on an earth-like terra-planet. *Earth System Dynamics*, **9 (2)**, 739–756, doi:10.5194/esd-9-739-2018.

Kang, S. M., 2020: Extratropical Influence on the Tropical Rainfall Distribution. **1**, 24–36.

Kang, S. M., I. M. Held, D. M. W. Frierson, and M. Zhao, 2008: The Response of the ITCZ to Extratropical Thermal Forcing: Idealized Slab-Ocean Experiments with a GCM. *Journal of Climate*, **21 (14)**, 3521–3532, doi:10.1175/2007JCLI2146.1.

Kim, J. E., M. M. Laguë, and A. L. S. Swann, 2020: Evaporative Resistance is of Equal Importance as Surface Albedo in High-Latitude Surface Temperatures Due to Cloud Feedbacks. 1–10, doi:10.1029/2019GL085663.

Kirschvink, J. L., 1992: Late Proterozoic low-latitude global glaciation: the snowball Earth. *The Proterozoic Biosphere*, **52**, 51–52, doi:10.1038/scientificamerican0100-68.

Kooperman, G. J., Y. Chen, F. M. Hoffman, C. D. Koven, K. Lindsay, M. S. Pritchard, A. L. S. Swann, and J. T. Randerson, 2018: Forest response to rising CO2 drives zonally asymmetric rainfall change over tropical land. *Nature Climate Change*, **8**, doi: 10.1038/s41558-018-0144-7.

Kuhlbrodt, T., and J. Gregory, 2012: Ocean heat uptake and its consequences for the magnitude of sea level rise and climate change. *Geophysical Research Letters*, **39 (18)**.

Kump, L. R., J. F. Kasting, R. G. Crane, and others, 2004: *The Earth System*, Vol. 432. Pearson Prentice Hall Upper Saddle River, NJ.

Laguë, M. M., G. B. Bonan, and A. L. S. Swann, 2019: Separating the Impact of Individual Land Surface Properties on the Terrestrial Surface Energy Budget in both the Coupled and Uncoupled Land–Atmosphere System. *Journal of Climate*, **32 (18)**, 5725–5744, doi:10.1175/jcli-d-18-0812.1.

Laguë, M. M., and A. L. S. Swann, 2016: Progressive Mid-latitude Afforestation: Impacts on Clouds, Global Energy Transport, and Precipitation. *Journal of Climate*, **29 (15)**, 5561–5573, doi:10.1175/JCLI-D-15-0748.1, URL http://dx.doi.org/10.1175/JCLI-D-15-0748.1.

Levins, R., 1966: The Strategy of Model Building in Polulation Biology. *American Scientist*, **5 (41)**, 420–431.

Loft, G., 1918: The Gulf Stream and the North Atlantic Drift. *Journal of Geography*, **17 (1)**, 8–17, doi:10.1080/00221341808984367.

Maher, P., and Coauthors, 2019: Model Hierarchies for Understanding Atmospheric Circulation. doi:10.1029/2018RG000607.

Manabe, S., 1969: Climate and the Ocean Circulation 1. *Monthly Weather Review*, **97 (11)**, 739–774, doi:10.1175/1520-0493(1969)097⟨0739:CATOC⟩2.3.CO;2, URL http://journals.ametsoc.org/doi/abs/10.1175/1520-0493(1969)097%3C0739:CATOC%3E2.3.CO;2.

Manabe, S., R. J. Stouffer, M. J. Spelman, and K. Bryan, 1991: Transient responses of a coupled ocean–atmosphere model to gradual changes of atmospheric CO2. Part I. Annual mean response. *Journal of Climate*, **4 (8)**, 785–818.

Manabe, S., and T. B. Terpstra, 1974: The effect of moutains on the general circulation of the Atmosphere. 3 pp.

Maroon, E. A., D. M. Frierson, S. M. Kang, and J. Scheff, 2016: The precipitation response to an idealized subtropical continent. *Journal of Climate*, **29 (12)**, 4543–4564, doi:10.1175/JCLI-D-15-0616.1.

Marshall, D. P., and L. Zanna, 2014: A conceptual model of ocean heat uptake under climate change. *Journal of Climate*, **27 (22)**, 8444–8465.

Marshall, J., and R. A. Plumb, 2008: *Atmosphere, ocean, and climate dynamics: an introductory text*, Vol. 93. Elsevier Academic Press.

McFarlane, N. A., 1987: The Effect of Orographically Excited Gravity Wave Drag on the General Circulation of the Lower Stratosphere and Troposphere. 1775–1800 pp., doi:10.1175/1520-0469(1987)044⟨1775:teooeg⟩2.0.co;2.

McMullin, E., 1985: Galilean idealization. *Studies in History and Philosophy of Science Part A*, **16 (3)**, 247–273.

Milly, P. C. D., and a. B. Shmakin, 2002: Global Modeling of Land Water and Energy Balances. Part I: The Land Dynamics (LaD) Model. *Journal of Hydrometeorology*, **3 (3)**, 283–299, doi:10.1175/1525-7541(2002)003⟨0283:GMOLWA⟩2.0.CO;2, URL http://journals.ametsoc.org/doi/abs/10.1175/1525-7541%282002%29003%3C0283%3AGMOLWA%3E2.0.CO%3B2.

Nilsson, J., P. L. Langen, D. Ferreira, and J. Marshall, 2013: Ocean basin geometry and the salinification of the atlantic ocean. *Journal of Climate*, **26 (16)**, 6163–6184.

North, G. R., J. G. Mengel, and D. A. Short, 1983: Simple energy balance model resolving the seasons and the continents: application to the astronomical theory of the ice ages. *Journal of Geophysical Research*, **88 (C11)**, 6576–6586, doi:10.1029/JC088iC11p06576.

Oke, T. R., 1987: *Boundary layer climates, Second edition*. doi:10.1017/CBO9781107415324.004.

Payne, R. E., 1972: Albedo of the Sea Surface. 959–970 pp., doi:10.1175/1520-0469(1972)029⟨0959:aotss⟩2.0.co;2.

Pietschnig, M., F. H. Lambert, M. Saint-Lu, and G. K. Vallis, 2019: The Presence of Africa and Limited Soil Moisture Contribute to Future Drying of South America. *Geophysical Research Letters*, **46 (21)**, 12 445–12 453, doi:10.1029/2019GL084441.

Queney, P., 1948: The Problem of Air Flow Over Mountains: A Summary of Theoretical Studies. *Bulletin of the American Meteorological Society*, **29 (1)**, 16–26, doi:10.1175/1520-0477-29.1.16.

Richardson, P. L., 1980: Benjamin Franklin and Timothy Folger's First Printed Chart of the Gulf Stream. *Science*, **207 (4431)**, 643–645.

Rose, B. E. J., K. C. Armour, D. S. Battisti, N. Feldl, and D. D. B. Koll, 2014: The dependence of transient climate sensitivity and radiative feedbacks on the spatial pattern of ocean heat uptake. *Geophysical Research Letters*, **41 (3)**, 1071–1078.

Sellers, P. J., and Coauthors, 1996: Comparison of radiative and physiological effects of doubled atmospheric CO2 on climate. *SCIENCE-NEW YORK THEN WASHINGTON-*, **271 (5254)**, 1402–1405, doi:10.1126/science.271.5254.1402.

Sellers, W. D., 1969: Global Climatic Model Based on the Energy Balance of the Earth- Atmosphere System. *Journal of Applied Meteorology*, **8 (3)**, 392–400.

Shukla, J., and Y. Mintz, 1982: Influence of Land-Surface Evapotranspiration on the Earth's Climate. *Science*, **215 (4539)**, 1498–1501.

Sikma, M., and J. Vilà-Guerau de Arellano, 2019: Substantial Reductions in Cloud Cover and Moisture Transport by Dynamic Plant Responses. *Geophysical Research Letters*, **46 (3)**, 1870–1878, doi:10.1029/2018GL081236.

Stocker, T. F., and Coauthors, 2013: Climate change 2013 the physical science basis: Working Group I contribution to the fifth assessment report of the Intergovernmental Panel on Climate Change. *Contribution of Working Group I to the Fifth Assessment Report of the Intergovernmental Panel on Climate Change.*, **9781107057**, 1–1535, doi:10.1017/CBO9781107415324.

Stouffer, R. J., S. Manabe, and K. Bryan, 1989: Interhemispheric asymmetry in climate response to a gradual increase of atmospheric CO2. *Nature*, **342 (6250)**, 660–662.

Sud, Y. C., J. Shukla, and Y. Mintz, 1988: Influence of Land Surface Roughness on Atmospheric Circulation and Precipitation: A Sensitivity Study with a General Circulation Model. 1036–1054 pp., doi:10.1175/1520-0450(1988)027⟨1036:iolsro⟩2.0.co;2.

Sutton, R. T., B. Dong, and J. M. Gregory, 2007: Land/sea warming ratio in response to climate change: IPCC AR4 model results and comparison with observations. *Geophysical Research Letters*, **34 (2)**, 2–6, doi:10.1029/2006GL028164.

Swann, A. L. S., I. Y. Fung, and J. C. H. Chiang, 2012: Mid-latitude afforestation shifts general circulation and tropical precipitation. *Proceedings of the National Academy of Sciences*, **109 (3)**, 712–716, doi:10.1073/pnas.1116706108.

Thomson, S. I., and G. K. Vallis, 2019: Hierarchical Modeling of Solar System Planets with Isca. *Atmosphere*, **10 (12)**, 803, doi: 10.3390/atmos10120803.

Trenberth, K. E., and J. M. Caron, 2001: Estimates of meridional atmosphere and ocean heat transports. *Journal of Climate*, **14 (16)**, 3433–3443.

Vallis, G. K., and Coauthors, 2018: Isca, v1.0: A framework for the global modelling of the atmospheres of Earth and other planets at varying levels of complexity. *Geoscientific Model Development*, **11 (3)**, 843–859, doi:10.5194/gmd-11-843-2018.

Voigt, A., 2013: The dynamics of the Snowball Earth Hadley circulation for off-equatorial and seasonally varying insolation. *Earth System Dynamics*, **4 (2)**, 425–438, doi:10.5194/esd-4-425-2013.

Voigt, A., D. Abbot, R. Pierrehumbert, and J. Marotzke, 2011: Initiation of a marinoan snowball earth in a state-of-the-art atmosphere-ocean general circulation model. *Climate of the Past*, **7**, 249–263.

Voigt, A., I. M. Held, and J. Marotzke, 2012: Hadley cell dynamics in a virtually dry snowball Earth atmosphere. *Journal of the Atmospheric Sciences*, **69 (1)**, 116–128, doi:10.1175/JAS-D-11-083.1.

Voigt, A., and Coauthors, 2016: The tropical rain belts with an annual cycle and a continent model intercomparison project: TRACMIP. *Journal of Advances in Modeling Earth Systems*, **8 (4)**, 1868–1891, doi:10.1002/2016MS000748.

Wallace, J. M., Y. Zhang, and J. A. Renwick, 1995: Dynamic Contribution to Hemispheric Mean Temperature Trends. *Science*, **270 (5237)**, 780–783.

Wei, H.-H., and S. Bordoni, 2018: Energetic Constraints on the ITCZ Position in Idealized Simulations With a Seasonal Cycle. *Journal of Advances in Modeling Earth Systems*, **10 (7)**, 1708–1725, doi: 10.1029/2018MS001313.

Wiscombe, W., and S. Warren, 1980: A Model for Spectral Albedo I: Pure Snow. 2712–2733 pp.

Wordsworth, R. D., 2016: The Climate of Early Mars. *Annual Review of Earth and Planetary Sciences*, **44 (1)**, 381–408, doi:10.1146/annurev-earth-060115-012355.

Worsley, T. R., and D. L. Kidder, 1991: First-order coupling of paleogeography and CO 2 , with global surface temperature and its latitudinal contrast. *Geology*, **19 (12)**, 1161–1164, doi:10.1130/0091-7613(1991)019⟨1161:FOCOPA⟩2.3.CO;2.

Yoshimori, M., and A. J. Broccoli, 2008: Equilibrium Response of an Atmosphere–Mixed Layer Ocean Model to Different Radiative Forcing Agents: Global and Zonal Mean Response. *Journal of Climate*, **21 (17)**, 4399–4423, doi:10.1175/2008JCLI2172.1, URL http://dx.doi.org/10.1175/2008JCLI2172.1.

Zarakas, C. M., A. L. Swann, M. M. Laguë, K. C. Armour, and J. T. Randerson, 2020: Plant Physiology Increases the Magnitude and Spread of the Transient Climate Response to CO2 in CMIP6 Earth System Models. *Journal of Climate*, 1–44, doi:10.1175/jcli-d-20-0078.1.

Zelinka, M. D., D. A. Randall, M. J. Webb, and S. A. Klein, 2017: Clearing clouds of uncertainty. *Nature Climate Change*, **7 (10)**, 674–678, doi:10.1038/nclimate3402.

LIST OF TABLES

Table 1. List of the idealized-continent Isca simulations used in this study, along with the land surface property values for each experiment. 50

TABLE 1. List of the idealized-continent Isca simulations used in this study, along with the land surface property values for each experiment.

Experiment name	**Description**	**Land albedo**	**Bucket depth [m H_20]**	**Initial water in bucket [m H_20]**
NorthlandBright	Northern hemisphere continent with an albedo brighter than the ocean.	0.325	0.15	0.1
NorthlandDark	Northern hemisphere continent with the same albedo as the ocean.	0.25	0.15	0.1
NorthlandEmpty	Like NorthlandBright, but initialized with no water on the land surface.	0.325	0.15	0
NorthlandDry	Like NorthlandBright, but with a very small capacity for the land to hold water.	0.325	0.00001	0
Lakeworld	All-land planet with bucket hydrology modified to allow lakes to form.	0.325	0.15	0.1
NorthWestLand	Single 180°-longitude wide continent from 0-90°N, covering 25% of the planet's surface. Land surface properties same as NorthlandBright.	0.325	0.15	0.1
NorthWestLandDry	Same as NorthWestLand, but with the same land surface properties as as NorthlandDry.	0.325	0.15	0.00001
ThreeQuarterLand	Single 270°-longitude wide continent from 0-90°N, covering 37.5% of the planet's surface. Land surface properties same as NorthlandBright.	0.325	0.15	0.1
ThreeQuarterLandDry	Same as ThreeQuarterLand, but with the same land surface properties as as NorthlandDry.	0.325	0.15	0.00001
TwoPatchLand	Two equally-spaced 90°-longitude wide continents from 0-90°N, covering a combined total 25% of the planet's surface. Land surface properties same as NorthlandBright.	0.325	0.15	0.1
TwoPatchLandDry	Same as TwoPatchLand, but with the land surface properties the same as NorthlandDry.	0.325	0.15	0.00001
ThreePatchLand	Three equally-spaced 90°-longitude wide continents from 0-90°N, covering a combined total 37.5% of the planet's surface. Land surface properties same as NorthlandBright.	0.325	0.15	0.1
ThreePatchLandDry	Same as ThreePatchLand, but with the land surface properties the same as NorthlandDry.	0.325	0.15	0.00001
Aqua	Aquaplanet simulation with 20m mixed layer (no land)	–	–	–

LIST OF FIGURES

Fig. 1. Maps of the continental distributions used in this study. Grey areas indicate land, while white areas indicate ocean. 53

Fig. 2. Zonal mean temperature (a,c) and precipitation (b,d). The NorthlandBright simulation is shown in (a) & (b) (solid lines). The anomalies for NorthlandDark - NorthlandBright (dashed lines) and NorthlandDry - NorthlandBright (dotted lines) are shown in (c) & (d). In a-d, black lines indicate annual mean values, while blue (red) show values for December/January/February (June/July/August) in (a,c) and cyan (magenta) show values for February/March/April (August/September/October) in (b,d). Shading in a-d indicates $\pm$ 1 standard deviation. Panels (e,f) show the annual mean change in zonal mean relative humidity (shading) and temperature (contours) for (e) NorthlandDark-NorthlandBright and (f) NorthlandDry-NorthlandBright. Temperature contours are spaced at 1K. Only humidity values in (e,f) which differ significantly ($p < 0.05$ using a student's t-test) are shown. 54

Fig. 3. Zonal mean seasonal cycle of (a) precipitation, (b) evaporation, and (c) precipitation-evaporation (P-E) for the spun-up NorthlandBright simulation; the equator/continental boundary is marked by the solid black line. Zonal mean terrestrial water storage over the first 6 simulation years for (d) NorthlandBright and (e) NorthlandEmpty. Zonal mean terrestrial water storage for (f) the full 80 year simulation of Lakeworld (note the non-linear color bar). Cyan contour in (f) at 150mm shows the bucket capacity (i.e. fully saturated soil moisture). 55

Fig. 4. Seasonal cycle of zonal mean precipitation from 40°S to 40°N in (a) NorthlandBright, (b) NorthlandDark, (c) NorthlandDry, and (d) Aqua. 56

Fig. 5. Change in the zonal mean surface energy budget for NorthlandDry - NorthlandBright over the course of the year. The change in net SFC *SW* is shown in (a) while the change in downwards LW is shown in (b). LW emitted by the surface is sown in (c), while (d) and (e) show sensible and latent heat, respectively. (f) shows the change in net surface energy uptake ($E_{in} = SW^{\downarrow} - SW^{\uparrow} + LW^{\downarrow}$), where positive values indicate more energy into the surface; in the annual mean this would be balanced by $E_{out} = LW^{\uparrow} + LH + SH$. 57

Fig. 6. Change in the zonal mean TOA energy budget for NorthlandDry - NorthlandBright over the course of the year. The change in net TOA *SW* is shown in (a) while the change in outgoing longwave radiation is shown in (b). The net TOA energy budget (a-b) is shown in (c). The change in the atmospheric energy source $F_{net} = TOA_{net} - SFC_{net}$ is shown in (d), where positive indicates more energy into the atmosphere. 58

Fig. 7. Bar graph showing the area-weighted annual mean change in (a) surface temperature and (b) latent heat flux globally (gray), over land only (green), and over the ocean only (blue), for each continental configuration. Small vertical black lines on each bar indicate 1 standard deviation. The magnitude of the temperature/latent heat flux change is noted above or below each bar. The total global land fraction for each simulation is noted along the bottom of each panel. 59

Fig. 8. Annual mean change in surface temperature (left), latent heat flux (center), and percent change in zonal mean specific humidity (right) for suppressing terrestrial evaporation in various continental configurations. Thick black lines show the continental boundary. 60

Fig. 9. Change in surface temperature (left), change in latent heat flux (center), and percent change in zonal mean specific humidity (right) between NorthlandDark and Aqua. The annual mean change is shown in a-c, while the zonal-mean seasonal cycle is shown in d-e. 61

Fig. 10. Relationship between the latitude of the ITCZ and the magnitude of cross-equatorial energy flux. The latitude of the ITCZ is calculated as the center of mass of precipitation between 30°S and 30°N; the magnitude of cross-equatorial energy flux is calculated as the magnitude of meridional atmospheric energy transport at the equator. Black markers indicate annual mean values, while blue, purple, green, and red markers indicate DJF, MAM, JJA, and SON averages, respectively. Circles show values for NorthlandBright, x for NorthlandDark, and triangles for Aqua. Each individual marker shows the seasonally averaged value for a single year of the time series. NorthlandDry is not included in the regression calculations here as the ITCZ effectively collapses over the continent. 62

Fig. 11. Zonally averaged net TOA energy flux (TOA, blue dotted line), net surface energy flux (SFC, green dash-dot line), and the atmospheric column energy source ($F_{net} = TOA - SFC$; black solid line) for the annual mean (top row), DJF (middle row) and JJA (bottom row). NorthlandBright is shown in the first column, NorthlandDark in the second, NorthlandDry in the third, and Aqua in the fourth. The total column integrated cross-equatorial atmospheric energy transport (postitive northwards) for each season is noted in the lower right of each panel. 63

Fig. 12. Schematic showing the possible surface temperature response to suppressed terrestrial evaporation for a variety of NH continental configurations. Land area generally increases from left to right, though for a given total land area, larger continents sit further to the right on the curve than smaller, more numerous continents. Qualitative locations of suppressing terrestrial evaporation on TwoPatchLand, NorthWestLand, ThreePatchLand, ThreeQuarterLand, and Northland are shown by the maps of temperature change for each continental configuration, with the annual mean change in land surface temperature noted on each map. . . . 64

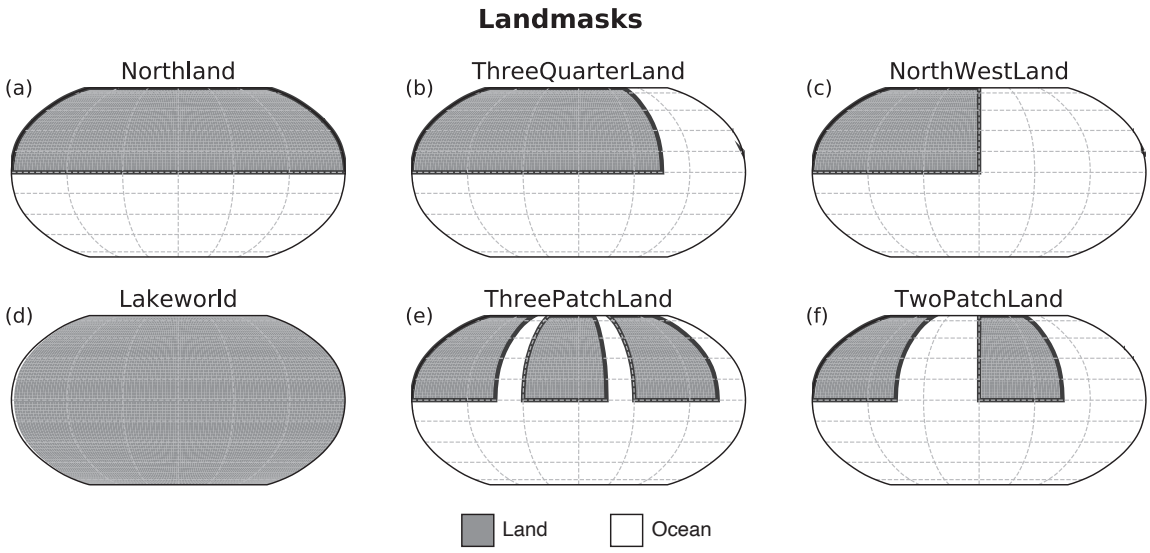

1130 FIG. 1. Maps of the continental distributions used in this study. Grey areas indicate land, while white areas
1131 indicate ocean.

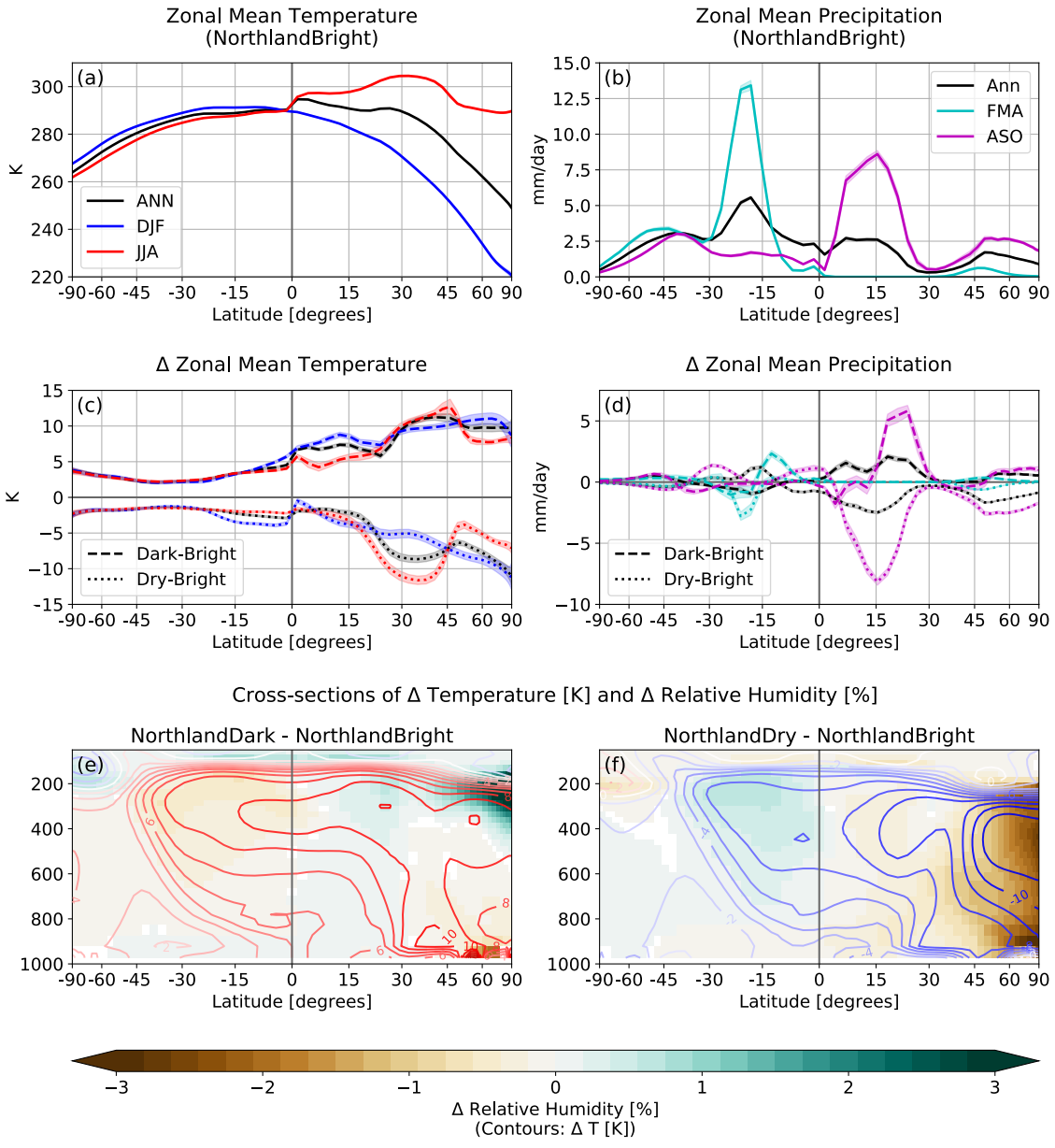

1132 FIG. 2. Zonal mean temperature (a,c) and precipitation (b,d). The NorthlandBright simulation is shown in
1133 (a) & (b) (solid lines). The anomalies for NorthlandDark - NorthlandBright (dashed lines) and NorthlandDry
1134 - NorthlandBright (dotted lines) are shown in (c) & (d). In a-d, black lines indicate annual mean values, while
1135 blue (red) show values for December/January/February (June/July/August) in (a,c) and cyan (magenta) show
1136 values for February/March/April (August/September/October) in (b,d). Shading in a-d indicates $\pm$ 1 standard
1137 deviation. Panels (e,f) show the annual mean change in zonal mean relative humidity (shading) and temper-
1138 ature (contours) for (e) NorthlandDark-NorthlandBright and (f) NorthlandDry-NorthlandBright. Temperature
1139 contours are spaced at 1K. Only humidity values in (e,f) which differ significantly ($p < 0.05$ using a student's
1140 t-test) are shown.

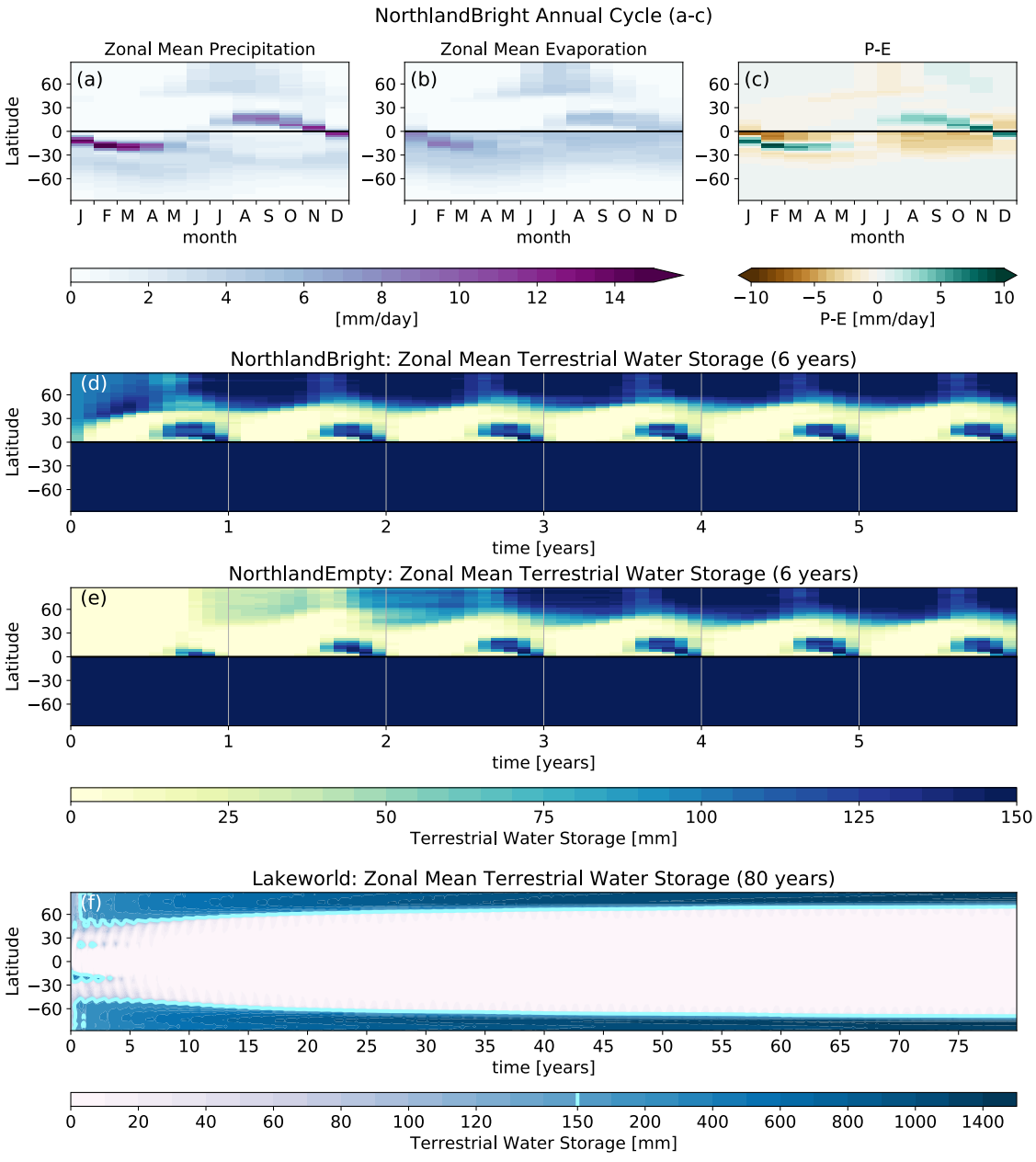

FIG. 3. Zonal mean seasonal cycle of (a) precipitation, (b) evaporation, and (c) precipitation-evaporation (P-E) for the spun-up NorthlandBright simulation; the equator/continental boundary is marked by the solid black line. Zonal mean terrestrial water storage over the first 6 simulation years for (d) NorthlandBright and (e) NorthlandEmpty. Zonal mean terrestrial water storage for (f) the full 80 year simulation of Lakeworld (note the non-linear color bar). Cyan contour in (f) at 150mm shows the bucket capacity (i.e. fully saturated soil moisture).

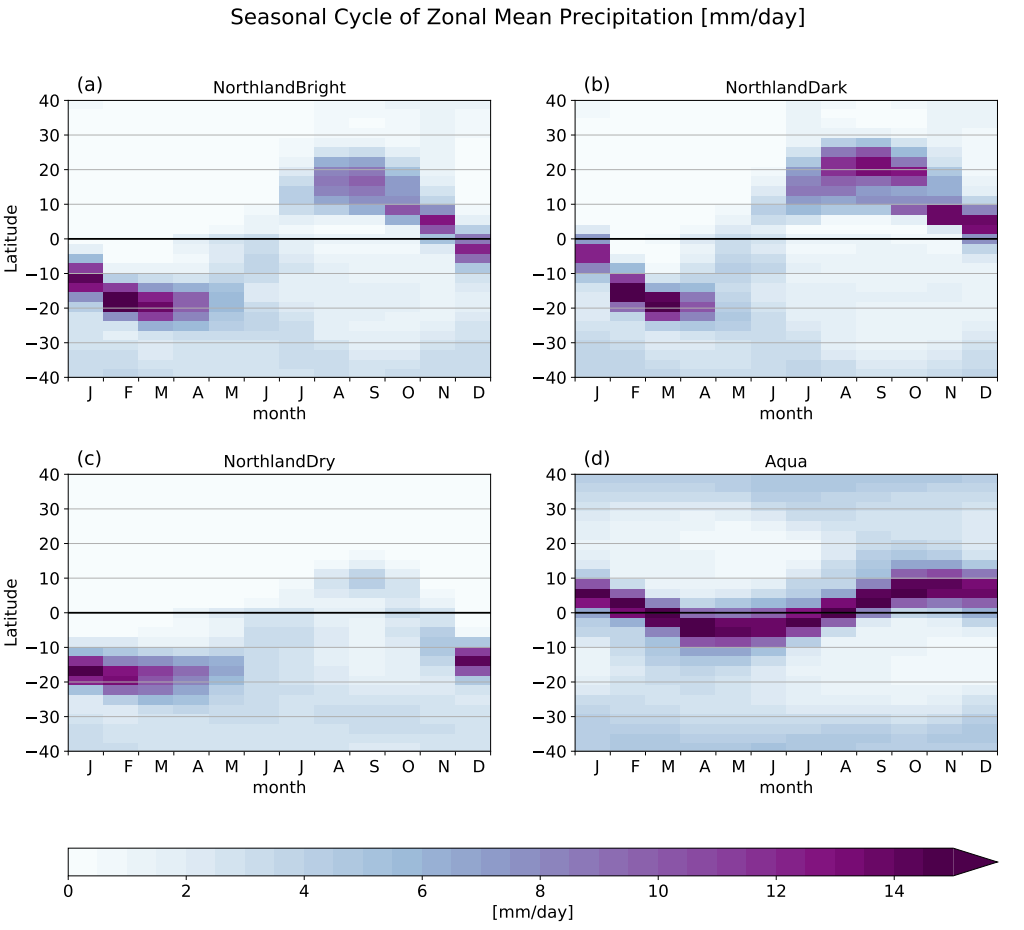

1147 FIG. 4. Seasonal cycle of zonal mean precipitation from 40°S to 40°N in (a) NorthlandBright, (b) Northland-
1148 Dark, (c) NorthlandDry, and (d) Aqua.

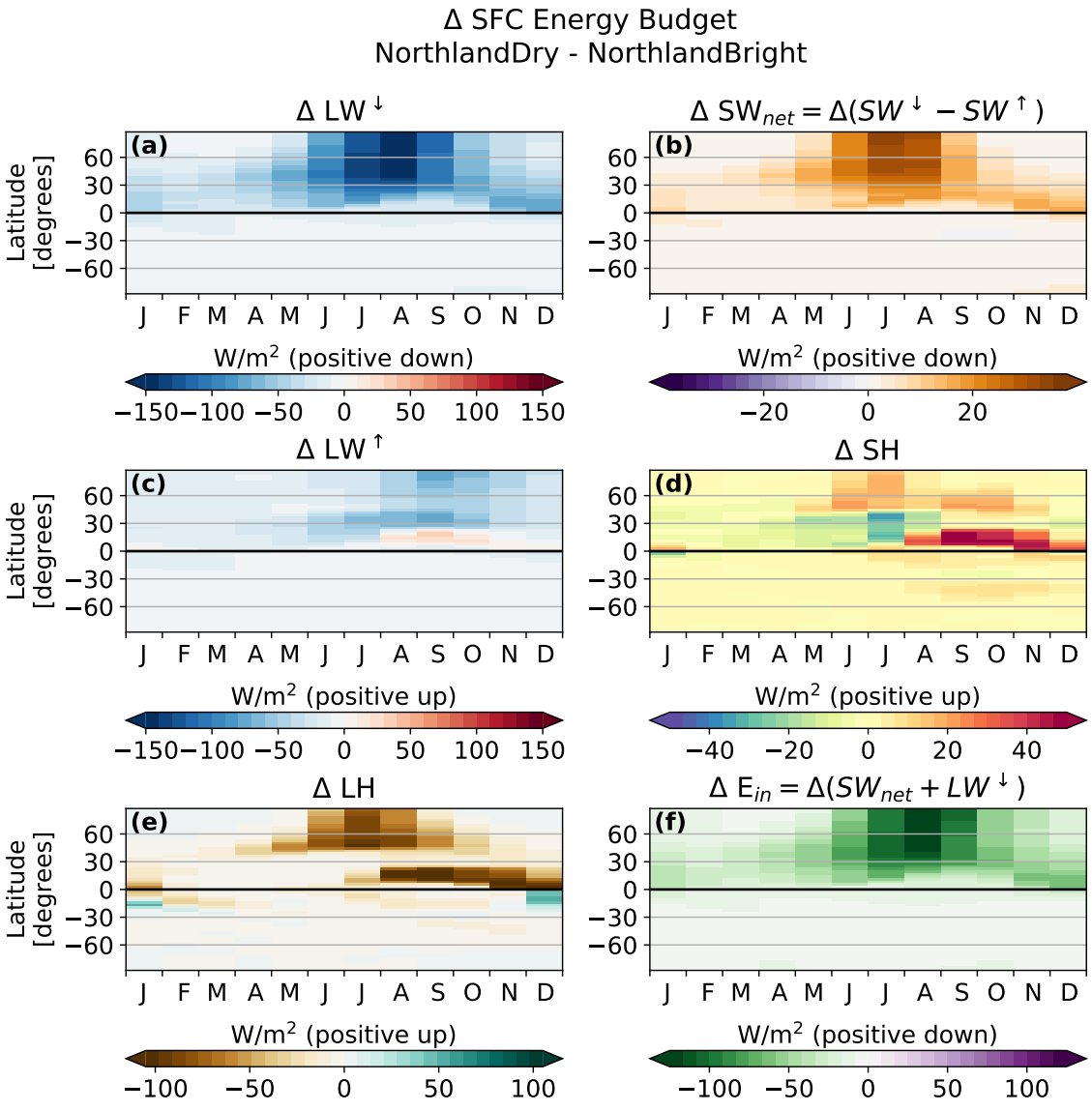

1149 FIG. 5. Change in the zonal mean surface energy budget for NorthlandDry - NorthlandBright over the course
1150 of the year. The change in net SFC SW is shown in (a) while the change in downwards LW is shown in (b). LW
1151 emitted by the surface is sown in (c), while (d) and (e) show sensible and latent heat, respectively. (f) shows the
1152 change in net surface energy uptake ($E_{in} = SW^{\downarrow} - SW^{\uparrow} + LW^{\downarrow}$), where positive values indicate more energy into
1153 the surface; in the annual mean this would be balanced by $E_{out} = LW^{\uparrow} + LH + SH$.

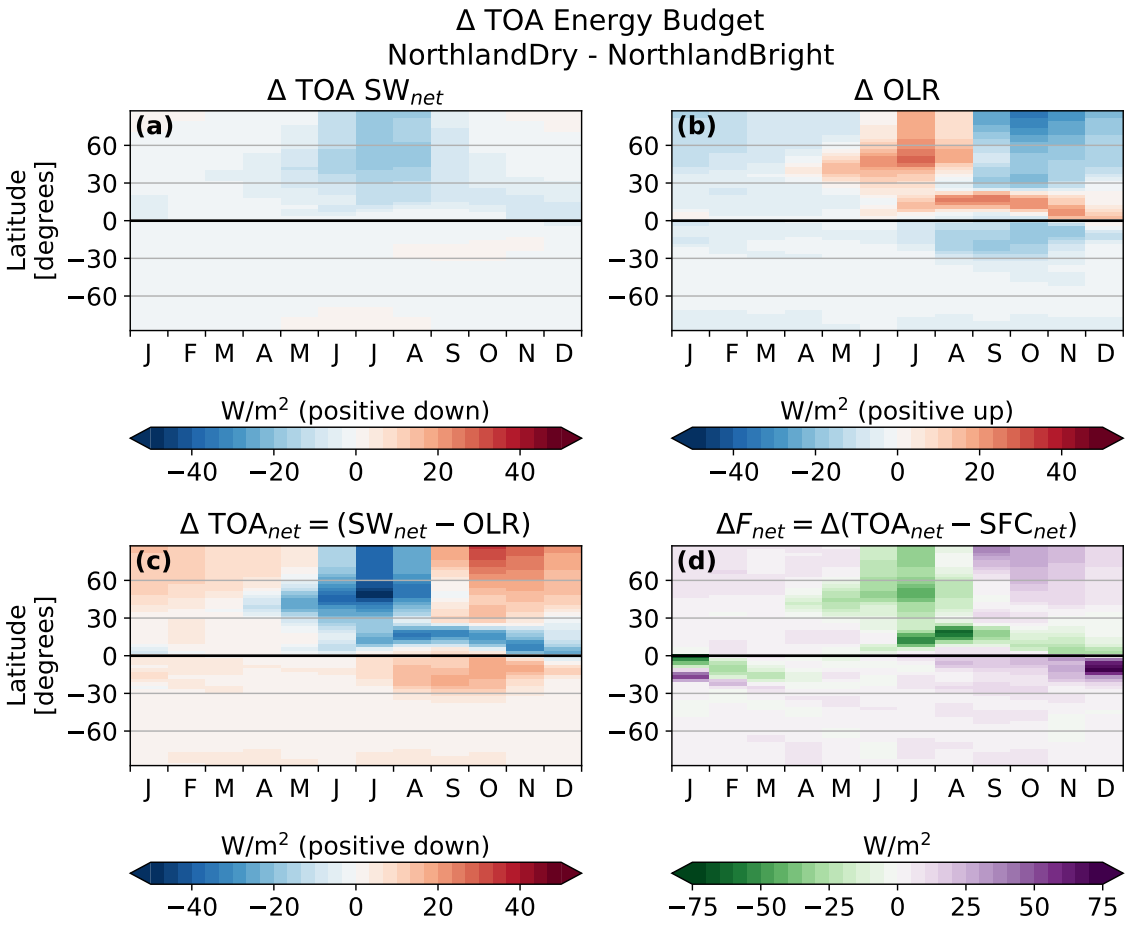

1154 FIG. 6. Change in the zonal mean TOA energy budget for NorthlandDry - NorthlandBright over the course
1155 of the year. The change in net TOA *SW* is shown in (a) while the change in outgoing longwave radiation is
1156 shown in (b). The net TOA energy budget (a-b) is shown in (c). The change in the atmospheric energy source
1157 $F_{net} = TOA_{net} - SFC_{net}$ is shown in (d), where positive indicates more energy into the atmosphere.

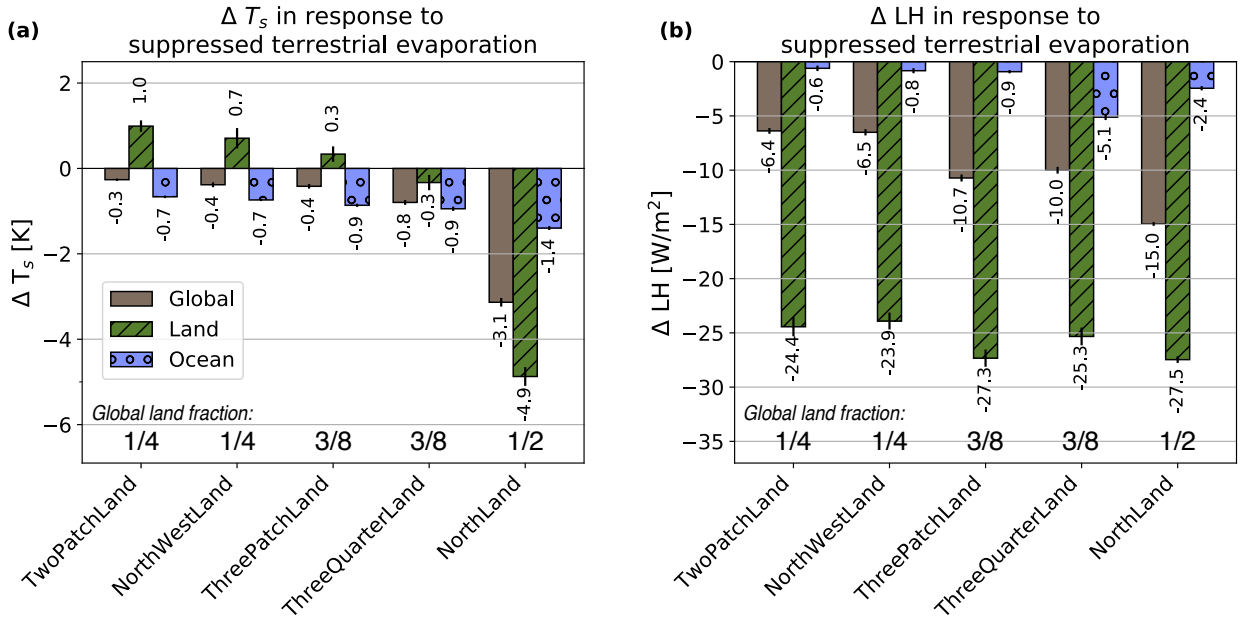

FIG. 7. Bar graph showing the area-weighted annual mean change in (a) surface temperature and (b) latent heat flux globally (gray), over land only (green), and over the ocean only (blue), for each continental configuration. Small vertical black lines on each bar indicate 1 standard deviation. The magnitude of the temperature/latent heat flux change is noted above or below each bar. The total global land fraction for each simulation is noted along the bottom of each panel.

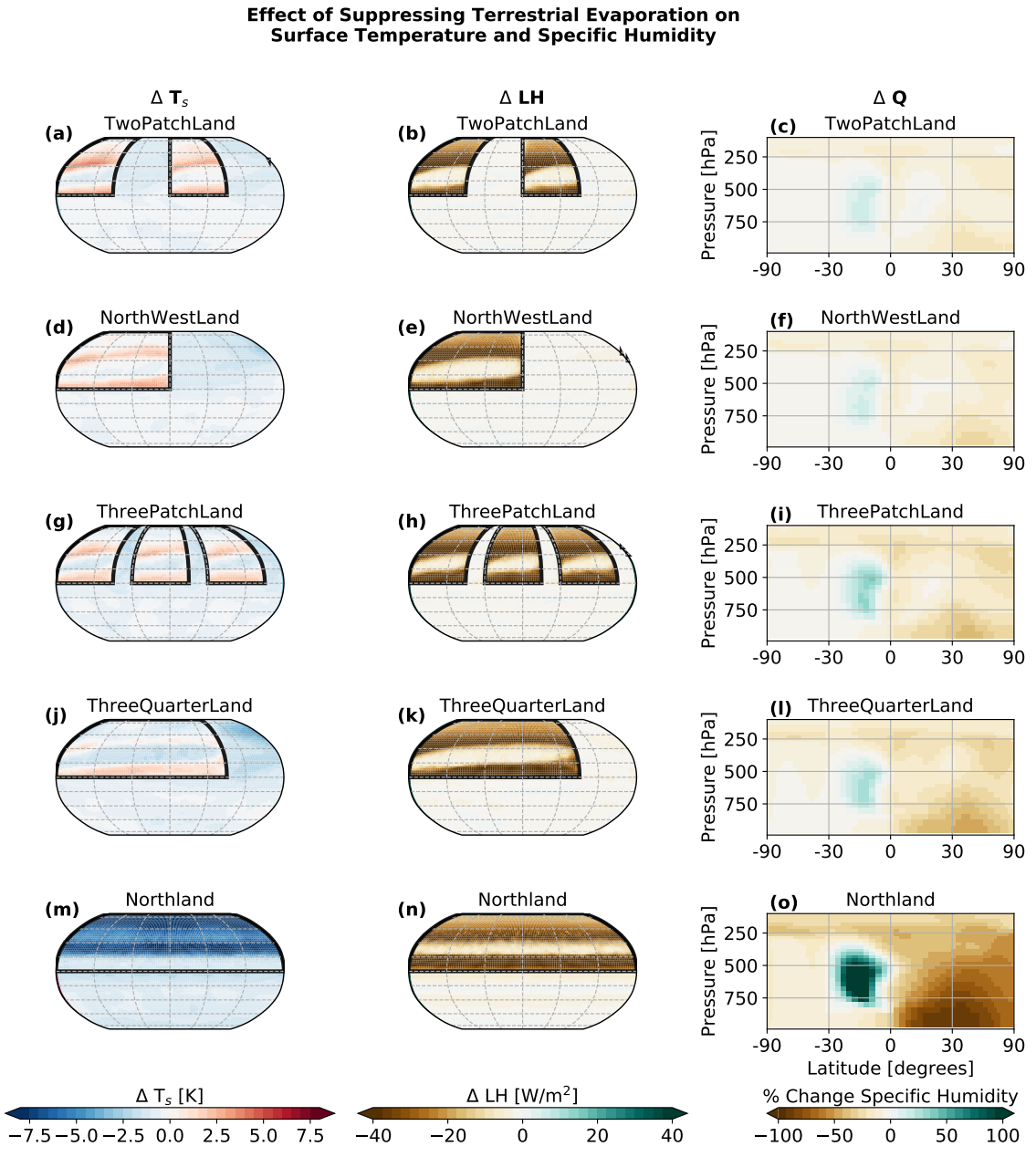

1163 FIG. 8. Annual mean change in surface temperature (left), latent heat flux (center), and percent change in
1164 zonal mean specific humidity (right) for suppressing terrestrial evaporation in various continental configurations.
1165 Thick black lines show the continental boundary.

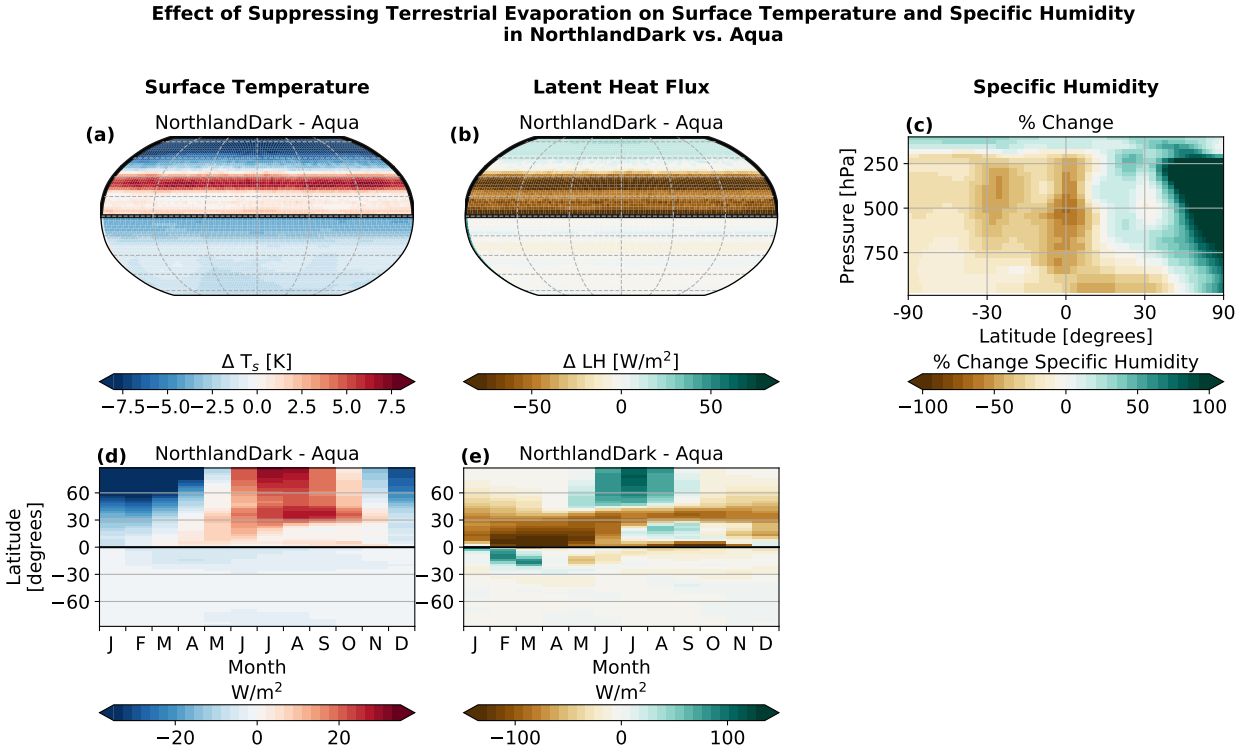

FIG. 9. Change in surface temperature (left), change in latent heat flux (center), and percent change in zonal mean specific humidity (right) between NorthlandDark and Aqua. The annual mean change is shown in a-c, while the zonal-mean seasonal cycle is shown in d-e.

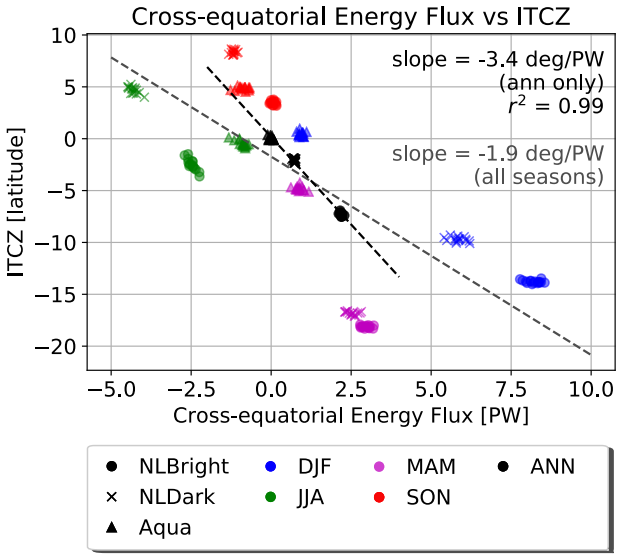

FIG. 10. Relationship between the latitude of the ITCZ and the magnitude of cross-equatorial energy flux. The latitude of the ITCZ is calculated as the center of mass of precipitation between 30°S and 30°N; the magnitude of cross-equatorial energy flux is calculated as the magnitude of meridional atmospheric energy transport at the equator. Black markers indicate annual mean values, while blue, purple, green, and red markers indicate DJF, MAM, JJA, and SON averages, respectively. Circles show values for NorthlandBright, x for NorthlandDark, and triangles for Aqua. Each individual marker shows the seasonally averaged value for a single year of the time series. NorthlandDry is not included in the regression calculations here as the ITCZ effectively collapses over the continent.

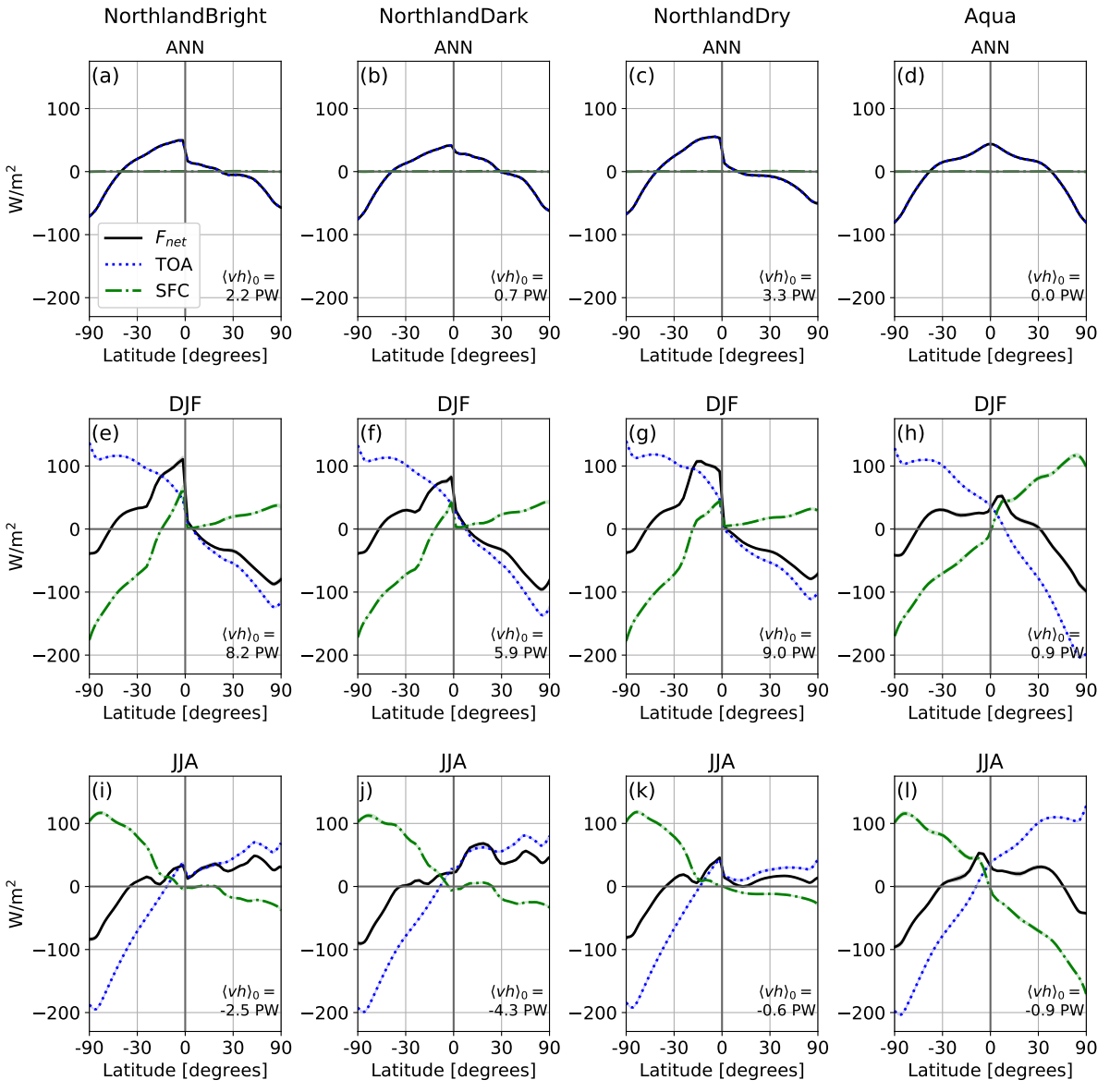

FIG. 11. Zonally averaged net TOA energy flux (*TOA*, blue dotted line), net surface energy flux (*SFC*, green dash-dot line), and the atmospheric column energy source ($F_{net} = TOA - SFC$; black solid line) for the annual mean (top row), DJF (middle row) and JJA (bottom row). NorthlandBright is shown in the first column, NorthlandDark in the second, NorthlandDry in the third, and Aqua in the fourth. The total column integrated cross-equatorial atmospheric energy transport (postitive northwards) for each season is noted in the lower right of each panel.

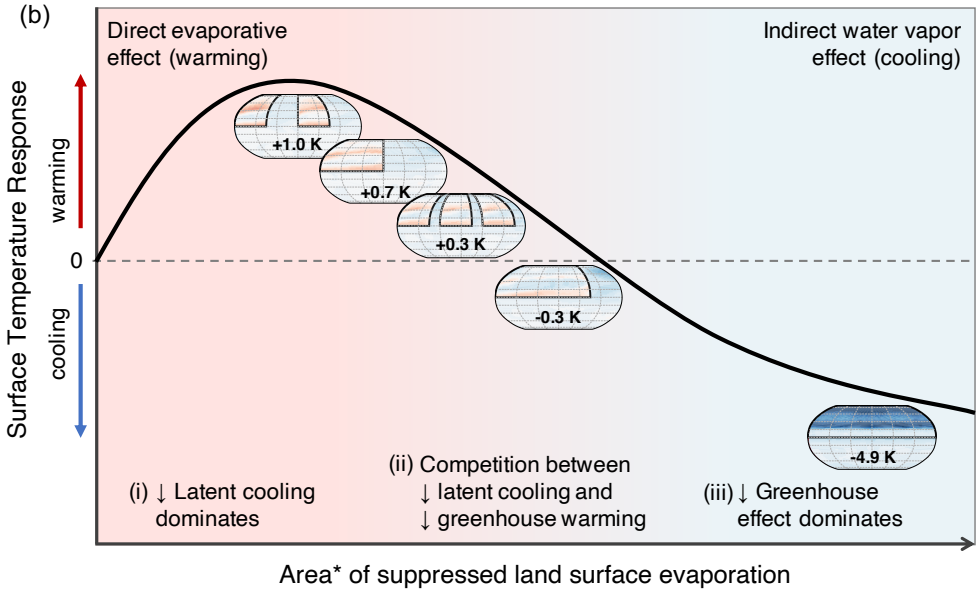

1183 FIG. 12. Schematic showing the possible surface temperature response to suppressed terrestrial evaporation
1184 for a variety of NH continental configurations. Land area generally increases from left to right, though for a
1185 given total land area, larger continents sit further to the right on the curve than smaller, more numerous conti-
1186 nents. Qualitative locations of suppressing terrestrial evaporation on TwoPatchLand, NorthWestLand, ThreeP-
1187 atchLand, ThreeQuarterLand, and Northland are shown by the maps of temperature change for each continental
1188 configuration, with the annual mean change in land surface temperature noted on each map.